AD-A207 581 NUMERICAL SIMULATION OF A TURBULENT FLOW THROUGH A SHOCK WAVE(U) NIELSEN ENGINEERING AND RESEARCH INC MOUNTAIN VIEW CA D NIXON ET AL. 21 APR 89 NEAR-TR-402 1/1

UNCLASSIFIED N00014-87-C-0483 F/G 20/4 NL

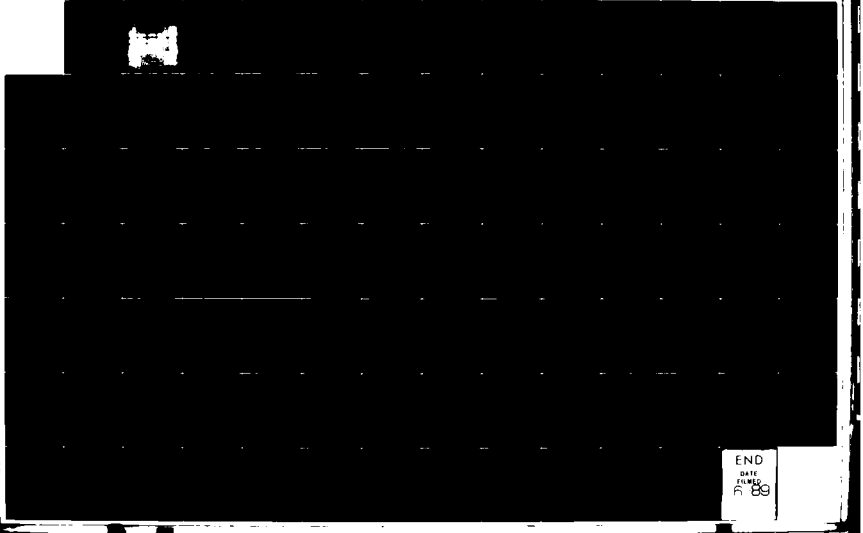

END
DATE FILMED
5 89

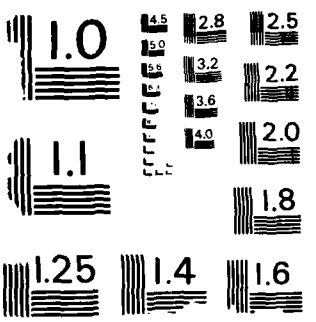
1.0
1.1
1.25
1.4
1.6
1.8
2.0
2.2
2.5
2.8
3.2
3.6
4.0
4.5
5.0
5.6

Numerical Simulation of a Turbulent Flow Through a Shock Wave

by
D. Nixon
G. Kuhn
M. Farshchi

NEAR inc
NIELSEN ENGINEERING AND RESEARCH, INC.

CC 5

4

Numerical Simulation of a Turbulent Flow Through a Shock Wave

by
D. Nixon
G. Kuhn
M. Farshchi

NEAR TR 402
April 1989

Final Report
Submitted Under Contract No. N00014-87-C-0483
to
Office of Naval Research
Arlington, Virginia

Nielsen Engineering & Research, Inc.
510 Clyde Avenue, Mountain View, CA 94043-2287
Telephone: (415)968-9457 • Fax: (415)968-1410

REPORT DOCUMENTATION PAGE

Form Approved
OMB No. 0704-0188

1a. REPORT SECURITY CLASSIFICATION Unclassified	1b. RESTRICTIVE MARKINGS
2a. SECURITY CLASSIFICATION AUTHORITY	3. DISTRIBUTION/AVAILABILITY OF REPORT Approved for public release; distribution is unlimited
2b. DECLASSIFICATION/DOWNGRADING SCHEDULE	
4. PERFORMING ORGANIZATION REPORT NUMBER(S) NEAR TR 402	5. MONITORING ORGANIZATION REPORT NUMBER(S)
6a. NAME OF PERFORMING ORGANIZATION Nielsen Engineering & Research, Inc. 6b. OFFICE SYMBOL (If applicable)	7a. NAME OF MONITORING ORGANIZATION Office of Naval Research
6c. ADDRESS (City, State, and ZIP Code) 510 Clyde Avenue Mountain View, CA 94043-2287	7b. ADDRESS (City, State, and ZIP Code) 800 North Quincy Street Arlington, VA 22217-5000
8a. NAME OF FUNDING/SPONSORING ORGANIZATION Office of Naval Research 8b. OFFICE SYMBOL (If applicable)	9. PROCUREMENT INSTRUMENT IDENTIFICATION NUMBER N00014-87-C-0483
8c. ADDRESS (City, State, and ZIP Code) 800 North Quincy Street Arlington, VA 22217-5000	10. SOURCE OF FUNDING NUMBERS PROGRAM ELEMENT NO. / PROJECT NO. / TASK NO / WORK UNIT ACCESSION NO.
11. TITLE (Include Security Classification) (U) Numerical Simulation of a Turbulent Flow Through a Shock Wave	
12. PERSONAL AUTHOR(S) G. Kuhn, D. Nixon	
13a. TYPE OF REPORT Final Technical 13b. TIME COVERED FROM 2/1/87 TO 1/31/89	14. DATE OF REPORT (Year, Month, Day) April 21, 1989 15. PAGE COUNT
16. SUPPLEMENTARY NOTATION	
17. COSATI CODES FIELD / GROUP / SUB-GROUP	18. SUBJECT TERMS (Continue on reverse if necessary and identify by block number) Shock Waves, Turbulence

19. ABSTRACT (Continue on reverse if necessary and identify by block number)

This report describes the results of research into the interaction between shock waves and turbulent flows using numerical simulations. The research was conducted at transonic speeds with a normal shock wave and two-dimensional turbulence, making use of existing knowledge and computational methods for developing insight to the shock/turbulence interaction. The results indicate that the shock has a significant effect on the turbulence. The shock produces a jump in the turbulence statistics, with a long relaxation distance to return to unshocked values. The turbulence kinetic energy is increased by as much as 30 percent by the shock. The density-velocity correlation becomes important during the shock jump and is greatly increased over the case without a shock. On the other hand, the pressure-velocity correlation is not so important. The shock speed and ripple were found to be important factors in determining the turbulence downstream of a shock wave. Shock

20. DISTRIBUTION/AVAILABILITY OF ABSTRACT ☒ UNCLASSIFIED/UNLIMITED ☐ SAME AS RPT ☐ DTIC USERS	21. ABSTRACT SECURITY CLASSIFICATION Unclassified
22a. NAME OF RESPONSIBLE INDIVIDUAL Dr. S. G. Lekoudis	22b. TELEPHONE (Include Area Code) (202)696-4405 22c. OFFICE SYMBOL

DD Form 1473, JUN 86 *Previous editions are obsolete.*

19. ABSTRACT (Continued)

speed and ripple correlations are the same size as other important turbulence correlations. The work must be extended to higher Mach numbers and three-dimensional turbulence, with oblique shocks and shear flows. The shock ripple may be more important for oblique shocks because of the larger v component.

Report

NUMERICAL SIMULATION OF A TURBULENT FLOW THROUGH A SHOCK WAVE

David Nixon
Gary D. Kuhn
Mohammad Farshchi
NIELSEN ENGINEERING & RESEARCH, INC.
510 Clyde Avenue
Mountain View, CA 94043-2287

21 April 1989

Final Report for Period 01 February 1987 - 31 January 1989

Approved for public release;
distribution unlimited.

Prepared for

OFFICE OF NAVAL RESEARCH
800 North Quincy Street
Arlington, VA 22217-5000

TABLE OF CONTENTS

Numerical Simulation of a Turbulent Flow
Through a Shock Wave

INTRODUCTION

Renewed interest in designing a hypersonic aircraft makes essential a reappraisal of the various fluid mechanics phenomena typical of such high speed flow. At hypersonic speeds there are flow phenomena that do not occur at subsonic speeds, such as real gas, chemical and thermal effects and, in particular, the effect on the flow of strong shock waves. Because of the extremely harsh environment in which these phenomena occur, it is difficult to investigate them experimentally and, consequently, a much greater reliance must be placed on numerical simulations than is the case in lower speed regimes.

This report describes the results of research conducted over a two-year period to provide a foundation for an extended research effort into the interaction between shock waves and turbulent flows at hypersonic speeds using numerical simulations. The work described herein was conducted at transonic speeds in order to make maximum use of existing knowledge and computational methods for developing insight to the shock/turbulence interaction and to aid in identifying problems in the overall approach.

One of the basic problems in high speed flow with shock waves is the shock/boundary layer interaction, particularly the interaction of the very large pressure gradient with the turbulence. The lack of detailed knowledge of this interaction is a probable cause of the frequent disagreement between numerical predictions of a shock/boundary layer interaction and experimental data from such interactions. Even if the shock/turbulence interaction itself were not the cause of inaccurate predictions, the uncertainty of the nature of the interaction precludes an accurate identification of the real cause. Consequently, it is essential to understand the nature of the shock/turbulence interaction.

It is expected that shock/turbulence interactions will be most important at hypersonic speeds where the shock is strongest. However, even a weak shock wave, typical of those at transonic speeds, should have a significant effect on the turbulence because of the very large pressure gradient across the shock. The first step in this investigation was, therefore, to study the interaction at these lower speeds, where the problem is more tractable, prior to attempting to study a hypersonic shock/turbulence interaction.

The primary objectives of the effort described herein were to choose a numerical scheme which would provide calculations of sufficient accuracy to give insight into shock/turbulence interactions, to allow extension of the work to higher Mach numbers and more complex flow configurations, and to define a flow configuration which could be used to study the interaction between turbulence and shock waves. The configuration needed to be physically realistic, but also simple enough to allow the identification of different aspects of the interaction. The numerical method chosen was an explicit, second order accurate, MacCormack scheme. The configuration chosen was a normal shock in a flow which was uniform except within a narrow region in the center of the computational domain. Calculations were performed in a supersonic flow with an upstream Mach number of 1.15. Turbulence was simulated in a finite portion of the entrance boundary using pseudo-random distributions of velocities, density, and pressure produced by a standard random number generator function. The shock wave was constrained to be held at a fixed position in the flow field by conditions imposed at the lateral boundaries. Calculations were performed for the turbulent flow with and without the shock. A statistical analysis was also performed by calculating samples of various statistical quantities as the calculations proceeded.

The remainder of this report will describe the selection of the numerical methods used, including tests of various computational grid configurations and the definition of the flow configuration. The particular grid and computer codes used will be described, along with the numerical methods of calculating statistical data from calculated turbulence. Results will be presented for a sample shock/turbulence interaction and for a separate analysis of a perturbed shock wave based on transonic indicial theory. The comparison of the two theories will be shown to

indicate that the motion of the shock wave due to turbulent fluctuations must be accounted for in order to accurately model the passage of turbulence through a shock.

NUMERICAL METHOD

The choice of a method of obtaining numerical solutions to the governing flow equations was made through considerations of the nature and complexity of the flow field to be calculated. Of primary concern was that the numerical method be easily applied to the problem of interest, and be easily modified and capable of extension to calculate fully three-dimensional flows. Of equal importance was the need for accuracy, both in time and space in order to be able to resolve rapid small scale fluctuations.

Since the calculations to be made were intended to provide information about the fundamental nature of the flow, the need for accuracy and ease of use of the method were also accompanied by the need for minimal artificial factors attributable to the numerical method itself. Examples of such artificial factors are artificial dissipation, shock smearing, that is, spreading of the shock over several computational points, and numerical oscillations. Also, the method must be able to calculate the correct shock speed and be well suited to a time accurate calculation. Finally, the computational method should be efficient, allowing many calculations to be made at minimum cost.

Three types of numerical methods were examined: artificial dissipation methods, linear hybridization methods, and Godunov methods. Artificial dissipation methods, such as generalized Lax-Wendrof methods, including MacCormack schemes, were found to be desirable because of simplicity of application. Such methods are especially successful when the artificial viscous effects can be mostly confined to a well-defined finite region, such as the high gradient region associated with a shock wave.

Linear hybridization methods, such as flux corrected transport or total variational diminishing (TVD) methods have the advantage of improved resolution of flow discontinuities when a uniform grid is used. However, the methods require

double the work of artificial dissipation methods and are clearly limited by the resolving power of the low order fluxes. Also, there is difficulty in devising appropriate weight factors for the low order and high order fluxes.

Godunov's approach avoids artificial dissipation and is highly accurate when a higher order difference scheme involving explicit nonlinearity is used. However, the use of a Riemann solver introduces a great deal of complexity into a difference scheme. Use of such a method for the problem of interest herein would involve a major code development, a formidable research program in itself. Such an approach was clearly unsuitable for the present study.

The computational method chosen for the present study was the explicit MacCormack scheme. The choice was based on three favorable characteristics of the method: (1) Simplicity; a two-dimensional scheme could be developed for preliminary work and could then be easily extended to three dimensions; (2) Relatively good resolution of unsteady shocks; (3) An estimate of implicit artificial dissipation is available, allowing an evaluation of the quality of the numerical results.

A two-dimensional Navier-Stokes solver was developed using the standard MacCormack scheme algorithm in a clustered cartesian coordinate system. An H-grid was chosen to avoid coordinate transformations for comparison of Reynolds stresses before and after shocks. The shock capturing performance of the code was tested by application to a flow field with an oblique shock. The results were compared to results obtained from a similar code developed by J. Shang (Ref. 1). Examples of the comparison of the two codes are shown in Figure 1. In Figure 1a and b plots of constant density contours for an oblique shock at freestream Mach number of 2.0 are shown. The code of Reference 1 is designated Code 1 in the figure, and the code developed in the present work is Code 2. Both codes produce similar solutions from the perspective given by the density contours. In Figure 1c and d, the density along a line through the shock wave is shown for the two codes. Clearly, both codes suffer somewhat from the coarseness of the grid and numerical dispersion effects. However, the new code produces a solution with reduced oscillations. The effects on the code's shock capturing performance of grid refinement, kinematic viscosity and second and fourth order artificial dissipation were tested, and results will be presented subsequently.

FLOW CONFIGURATION

In choosing a configuration for calculations of shock wave turbulence interactions, it was decided initially that a flow field was required that would allow observation of the direct effect of the shock wave on the turbulence and, conversely, of the turbulence on the shock. The flow field should be clearly defined and allow the researcher as much control as possible over the essential elements of the flow through manipulation of the inflow, outflow, and boundary conditions. Thus, it was considered important to avoid such things as: curved geometry, which would require a curvilinear coordinate system; oblique shocks, which would possibly undergo bifurcation, thus obscuring the effects of interest; shock reflections from boundaries, which would create a complex flow field, thus making more difficult the interpretation of shock-turbulence interaction effects; and no-slip boundary conditions which would create a shear flow and lead to development of a more complex field of turbulence.

The first configuration chosen for examination was a flow in a duct with a bump on one wall. The incoming flow was subsonic, and a transpiration condition was to be applied to the lower wall to generate a normal shock, with a symmetry condition at the upper boundary. The exit flow would also be subsonic. Unfortunately, such a configuration violates several of the criteria mentioned previously as to be avoided. For example, the boundary condition on the streamwise velocity component on the lower boundary is a no-slip condition. In addition to the creation of shear, such a condition leads to slow numerical convergence because of the grid refinement required for proper resolution of the near-wall flow. The no-slip condition was necessary because the equations being solved were the full Navier-Stokes equations. If the equations could have been reduced to the Euler equations by neglecting the viscous terms, the no-slip condition would not have been necessary. However, it was considered important to include the viscous terms since the flow was expected to be subject to viscous dissipation. Another fault of the duct flow configuration was that the shock wave location was not precisely controllable, nor was the shock perfectly normal, even without turbulence. Finally, the shock/turbulence interaction region was not clearly defined. All these considerations led to rejecting the duct-with-a-bump as the configuration of

choice, at least for the preliminary study. In retrospect, some of the objectionable conditions were found to exist to some degree in the configuration that was actually used, so that the duct-with-a-bump, or flow over an airfoil, remains a possibility for further study.

The configuration which was used was a simpler one in which the walls of the duct were removed, and a normal shock wave was created in a uniform flow field which contained turbulence in a central region. The incoming flow was slightly supersonic (M = 1.15). Inviscid boundary conditions were used at the top and bottom boundaries. The initial flow field was specified as a uniform flow with a normal shock, thus modeling a flow in a shock tube in which the observer is moving with the shock. The location of the shock was fixed in space by keeping the solution at the top and bottom boundaries constant and specifying the pressure at the downstream boundary to be the theoretical pressure for a normal shock from one-dimensional Rankine-Hugoniot theory. Some refinement of the solution was achieved by running a steady flow solution in which the incoming flow was constant, and the top and bottom boundary conditions were periodically revised by setting the flow variables equal to their values at the centerline. In this way, after several adjustments, a steady flow field was achieved which was the same everywhere, including the boundaries, with a shock jump which spread over several grid points in the streamwise direction, the number of grid points depending upon the magnitude of the real and artificial viscosities.

The generation of turbulence in the flow field will be discussed in a subsequent section. It is noted that the turbulence was specified in a central section of the inflow boundary. Disturbances from the turbulent flow field propagated along Mach lines toward the top and bottom boundaries of the configuration. The width of the computational space was such that these disturbances intersected the shock wave before they intersected the boundaries. Thus, the boundary conditions should represent realistically the steady propagation of a shock wave in a uniform flow field encountering a finite region of turbulence with the observer moving along with the undisturbed shock wave.

The development of the flow field in the steady case can be seen in Figures 2 and 3. In Figure 2, the convergence history of the maximum change in the numerical solution is shown. When the boundary conditions change, every 200 time

steps, there is a jump in the residual, which then proceeds to approach an asymptote. The asymptotic level is reduced each time the boundary conditions are refined. After four such refinements, as shown in the figure, the residual remained constant. It is noted that the particular numerical scheme being used in these calculations was an explicit MacCormack scheme, for which the asymptotic value of the residual is a function of the time step. Use of an implicit formulation would eliminate this effect. In Figure 3, the profile of the Mach number variation through the shock wave is shown. The effects of second and fourth order artificial dissipation and of Reynolds number are indicated. The first case is a Reynolds number of 10,000 and no artificial dissipation. The results shown in Figure 3a indicate that the shock is spread over about 6 grid points, and the numerical scheme produces some oscillations both upstream and downstream of the shock jump. In Figure 3b some second order dissipation has been added, producing no discernible change in the solution. Adding some fourth order dissipation alone, on the other hand, reduces substantially the oscillations downstream of the shock while leaving unaffected, or possibly slightly increasing, the upstream oscillations (Fig. 3c). Including both second and fourth order dissipation apparently is no better than the second order alone, as indicated in Figure 3d. Reynolds number effects are quite large as shown in Figure 3e and f, where the Reynolds number varies by an order of magnitude above and below that of Figure 3d. The higher Reynolds number (lower viscosity) clearly reduces the spreading of the shock over the grid, but increases the amplitude of the oscillations. The lower Reynolds number increases the spreading and reduces the oscillation amplitude.

Clearly, the choice of the parameter values which govern the quality of the numerical solution is the set of values which give the best resolution of the shock jump with the least oscillations for a given Reynolds number. The choice of Reynolds number is somewhat arbitrary. However, considerations of the desire to resolve a wide range of scales of turbulence lead to a value which allows the shock to be captured in as few points as possible commensurate with the minimization of the oscillations. With these considerations, both second and fourth order dissipation parameters were used for subsequent calculations, with Re = 10,000.

GRID DEFINITION

The computational grid used in preliminary calculations was uniform in the lateral directions (parallel to the shock wave) and exponentially stretched in the streamwise direction downstream of the shock. While this grid configuration allowed the efficient development of the computational techniques for producing a turbulent flow and computing statistics, accuracy in calculating the turbulence required a uniform grid since that would allow the minimum resolvable scales to be the same over the entire computational space. A uniform grid was therefore used in all subsequent calculations.

The computational space is shown in Figure 4. For most of the calculations, the grid dimensions were 0.1 x 0.1 with each axis divided into 80 segments. Some calculations were made with a 160x160 point grid to test the effect of the grid. The x axis defines the flow direction, the y axis defines the lateral direction. The flow enters the computational space from the left, at $x = 0$. The region where turbulence is introduced is along the y axis in the center of the inflow boundary.

STATISTICAL ANALYSIS

Understanding a turbulent flow requires examination of several kinds of data. Instantaneous as well as statistical information can provide useful insights. Statistical quantities can include a wide variety of data, from simple averages of quantities measured (or calculated) at a single point in space or time to correlations of quantities measured at several points and combinations of space and time. In this investigation, the statistical analysis of the flow dealt primarily with instantaneous velocity, pressure and density distributions, and statistical averages of velocity, pressure and density fluctuations, and products of fluctuations defined at a point. Some two-point correlations in both time and space were also calculated.

Basic statistical quantities were calculated by averaging over a specified ensemble of grid points and time steps. The main requirement of the statistical analysis is that the quantities included in the ensemble be independent. The turbulence under study was produced by an input distribution of quantities

randomly distributed in time and along the y axis at the inflow boundary. The solution generated by this inflow was assumed to be homogeneous with respect to variations in the y direction within a range defined by the specified inflow. The basic statistical ensemble at each x station was defined to consist of data at grid points along lines parallel to the y axis for all time steps. In order to avoid edge effects, of N grid points included in the inflow turbulence specification, N-4 points were included in the statistical ensemble. Statistical quantities were defined by

$$\langle f \rangle = \frac{1}{LT} \int_0^L \int_0^T f(x,t)\,dx\,dt \tag{1}$$

or, for a finite numerical ensemble,

$$\langle f \rangle = \frac{1}{N(J-2)} \sum_{j=2}^{J-1} \sum_{n=1}^{N} f_{jn} \tag{2}$$

where f is a quantity of interest, i.e., u, v, p, ρ, uv, pu, ρu, etc., J is the number of y-axis points at which the turbulence is introduced at the inflow boundary, and N is the number of time steps included in the ensemble. Values of all four basic flow quantities, u, v, p, ρ were accumulated at 36 y values between y = 0.025 and 0.075 in order to maximize the amount of data.

REPRESENTATION OF TURBULENCE

Turbulence is defined as an irregular condition of flow in which the various quantities show a random variation with time and space coordinates, so that statistically distinct average values can be discerned (Ref. 2). Frequently "pseudo-turbulence" is used, referring to a flow field with a regular pattern that shows a distinct constant periodicity in time and space, but produces certain statistical properties of a turbulent flow. In recent numerical simulation studies of turbulence, a typical technique is to begin a time-dependent solution of the Navier-Stokes

equations with a flow field with fluctuations of the velocities produced by various kinds of "pseudo-random" number generators (Ref. 3). After some integration time, it is found that the solution has evolved into a state that resembles an actual turbulent flow.

In the present study, the realistic simulation of turbulence was of less importance than the accuracy of the computational method and the definition of a flow configuration that would allow shock/turbulence interaction effects to be discerned. In the first place, the preliminary flow configuration was two-dimensional, thus precluding realistic simulation of a three-dimensional field of turbulent fluctuations. Secondly, it was not desirable to devote effort to perfecting the turbulence simulation until the fundamental value of the overall approach could be demonstrated.

As a preliminary method of simulating a turbulent flow field, the two velocity components, and the pressure and density were prescribed at each point of a range of y values at the inflow boundary using a series of numbers produced by a standard random number generator which produced pseudo-random values with a Gaussian distribution between 0 and 1. These numbers were then modified to produce some correlation between the values at successive time steps by the expression

$$S_n = CS_{n-1} + (1 - C^2)^{\frac{1}{2}} R_n \qquad (3)$$

where R_n is the sequence of independent random numbers, S_n is the next value of the correlated sequence, S_{n-1} is the previous value, and C is the correlation coefficient. In this work, the correlation coefficient was taken to be

$$C = 0.98 \qquad (4)$$

This value was somewhat arbitrarily chosen so that the autocorrelation of the S_n sequence decreases to 0.5 in about 30 time steps. These quantities were then used to define fluctuations of the flow field by the relations

$$\rho = \rho_\infty (1 + aS_n^1) \tag{5}$$

$$u = u\ (1 + bS_n^2) \tag{6}$$

$$v = u_\infty c S_n^3 \tag{7}$$

$$p = p_\infty (1 + dS_n^4) \tag{8}$$

where the superscript on the random sequence identifies a different sequence for each variable, each sequence independent from the others. It is recalled that these expressions are applied as a function of time at each point in a range of y values at the inflow boundary. Thus, while the time variation of the fluctuations at each y location is not completely random because of the correlation coefficient, C, the y variation is more random due to the relative independence of the terms of the R_n sequence. A simple three point smoothing was applied to the inflow conditions in the y-direction to help eliminate numerical problems created by large changes between the specified values of the flow variables at adjacent y locations in the incoming flow.

RESULTS FOR NORMAL SHOCK/TURBULENCE INTERACTIONS

Calculations were performed for three cases. First, the solution for a uniform steady flow with a shock wave was calculated. This provided the initial conditions for the next case, a flow with turbulence specified as described previously using random numbers in a finite region, forming a "jet" of turbulent flow in the center of the uniform flow. The side boundary conditions for that flow were the conditions at the final time step of the non-turbulent flow. Thus, the converged steady flow solution provided both the initial conditions and the boundary conditions for the subsequent turbulent solution. It also provides an estimate of the error associated with the numerical procedure. The third case calculated was a flow like the second case except that the flow was uniform everywhere initially, with supersonic inflow as in both previous cases, but with no shock jump on the side boundaries and with all independent variables, including the downstream pressure,

calculated by extrapolation at the downstream boundary. The second and third cases thus provided a comparison between a turbulent flow in a supersonic stream and a turbulent flow passing through a shock wave.

The calculated variables were normalized with respect to free stream quantities, with the resulting steady state conditions at the inflow boundary as follows:

$$u_\infty = 1.15$$
$$v_\infty = 0.0$$
$$\rho_\infty = 1.0$$
$$p_\infty = 1/\gamma$$

for

$$\gamma = 1.4$$

The Mach number distribution for the steady solution has already been shown in Figure 3d. The corresponding pressure distribution is shown in Figure 5. Typical inflow perturbations are shown in Figure 6. In Figure 6a, the ρ and ρu fluctuations as a function of time at the centerpoint of the inflow boundary are presented, while in Figure 6b the variation with y at a typical time step is shown. An indication of the effect of viscosity on the turbulence is shown in Figure 7 where the y variation of ρ and ρu at an x-station near the shock wave is seen to be considerably smoother than at the inflow boundary. The primary features of the previous plot are still discernible at this station, but the smaller features are smoothed a great deal.

For the analysis of turbulence, the statistical averages of fluctuating quantities are obtained by subtracting the mean values. For any collection of values of a function, the mean value is defined by Equation (1) or Equation (2). By definition, then, the average of the fluctuations about the mean value is zero. That is,

$$\langle f' \rangle = \langle f - \langle f \rangle \rangle = 0 \qquad (9)$$

Thus, products of fluctuating quantities can be calculated as follows

$$\langle f'g' \rangle = \langle (f - \langle f \rangle)\ (g - \langle g \rangle) \rangle = \langle fg \rangle - \langle f \rangle \langle g \rangle \qquad (10)$$

In these definitions, it is important to note that the mean value defined by Equation (2) depends upon the number of values used in the calculation. Also, the presence of serial correlation, or dependence between successive terms of a random sequence, can produce a bias in a finite sequence. Given a mean flow and random fluctuations about the mean, it is possible to achieve an average value for the mean flow-plus-fluctuations that equals the given mean flow within a finite uncertainty. The uncertainty can be reduced to a small value, but can never be zero. In test calculations with random numbers, it was concluded that at least 10^5 samples were needed to achieve an acceptable level of uncertainty. For example, Figure 8 shows the mean velocity fluctuation as given by Equation (2) with the individual values given by the random function part of Equation (6). The mean is presented as a function of the number of values in the ensemble for up to 10^5 points. The figure shows that for ensembles containing less than 50,000 points, the mean value is strongly dependent upon the size of the ensemble. For larger ensembles, the mean value approaches zero, but still can fluctuate considerably. For the calculations performed on the 80x80 grid in this work, values of the flow quantities were taken from 36 y locations at each time step. To assure a reasonable accuracy in the statistics, a total of 8000 time steps were calculated, making 288,000 values available for analysis. Test calculations for 2000 and 4000 time steps produced results in close agreement with the longer runs.

Some of the statistics of the calculated turbulence are shown in Figure 9-12. In Figure 9, the turbulence intensities, i.e., the rms values of the fluctuations in the u and v velocity components, are shown. The calculated distributions of the quantities for the cases with and without a shock wave are superimposed. Upstream of the shock, both solutions are identical, whereas downstream of the shock, there are measurable differences. Both the streamwise (normal to the shock) and the spanwise (parallel to the shock) turbulence intensity components appear to be slightly increased upon passage through the shock. The large spike in the intensities at the location of the shock is related to the shock capture region. In

general, the shock region is a nonconservative region in which the numerical solution is meaningless, and, accordingly, no special significance should be attached to the shock capture region, but only to the beginning and end points of the region (Ref. 4). This suggests that the shock capture region in Figures 9-12 can be ignored for the present analysis. The extent of the shock capture region is best determined by examining the variation of the mean flow through the shock. The distribution of the mean pressure, shown in Figure 13, indicates that the shock region consists of seven grid points, ranging from x = 0.0275 to x = 0.0350. The turbulence intensities shown in Figure 9 undergo large fluctuations in the shock region and do not return to the shock-free variation after the shock. The increase in the turbulence intensity downstream of the shock is considered to be due to the interaction between the shock wave and the turbulence. Figure 10 shows that there is also a density effect and a small effect on the pressure fluctuations, while Figure 11 indicates that the turbulence kinetic energy is increased by the shock wave and Figure 12 shows an increase in the product $<\rho' u'>$ from slightly negative ahead of the shock wave to 0.0003 downstream of the shock, with a slightly smaller magnitude effect on the product $<p' u'>$.

In view of the smallness of the numerical values of the changes in the density-velocity products and the turbulence kinetic energy, a note about the accuracy of the numerical calculations is in order. The algorithm used for the calculations is formally of second order accuracy. This means that the solution error is of the order of $(\Delta x)^2$, or, for the grid used in the calculations shown in Figures 9-13, the order of 10^{-6}. Another way to assess the accuracy of the calculations is to examine the solution for the case where no turbulence was present. In this example, the exact solution is known and the effect can be easily estimated by comparison of the computed and theoretical results. The variation of the numerical solution for the pressure variation along the centerline of the computational region was shown in Figure 5. The oscillations shown in that figure are due to the numerical scheme, and are the response to the shock discontinuity. Another source of error of interest in this analysis is the random error associated with the numerical calculations. This error can be quantified by applying the statistical calculations to the steady flow case. The error is indicated by the size of the "turbulent intensity" or rms fluctuation of the solution about the mean. The results for the rms velocity

components and the rms pressure and density fluctuations are presented in Table I. The results indicate that the maximum error outside the shock capture region is approximately $5x10^{-5}$. Recall that the rms fluctuations as indicated in Figures 9 and 10 are of the order of $5x10^{-2}$, three orders of magnitude larger. The variation of the mean velocities, density, pressure, and mass flux for the steady flow case is listed in Table II, along with the theoretical values for a normal shock wave. The maximum errors in the mean quantities occur near the shock due to the oscillations of the numerical scheme.

Consider now the velocity and density product. If each quantity is taken to be composed of an exact mean value, an error, and a turbulent fluctuation, that is

$$u = u_o + u_e + u' + u_e' \tag{11}$$

$$\rho = \rho_o + \rho_e + \rho' + \rho_e' \tag{12}$$

where $( )_o$ = the exact solution

$( )_e$ = *the error*

and

$( )'$ = the turbulent fluctuations, then the mean values over the entire ensemble of values calculated are

$$\langle u \rangle = u_o + \langle u_e \rangle \tag{13}$$

and

$$\langle \rho \rangle = \rho_o + \langle \rho_e \rangle \tag{14}$$

and

$$\langle \rho u \rangle - \langle \rho \rangle \langle u \rangle = \langle \rho' u' \rangle + \text{Error} \tag{15}$$

where

$$\text{Error} = \langle \rho_e u' \rangle + \langle \rho' u_e \rangle \tag{16}$$

The largest error in u_e' is due to the oscillations from the shock capture. These oscillations are spatial and are relative to the shock. If the shock does not move, then there is no contribution to u_e'. If the shock does move, then the maximum error can be estimated by assuming the error, E, is proportional to the magnitude of the oscillations, E_o, and is given by

$$E = 2E_o \, \delta X_s / \Delta X$$

where δX_s is the shock movement and ΔX is a grid cell; the wavelength of the oscillation is $2\Delta X$. Taking the rms. value of δX_s as a guide, and noting that

$$E \simeq 2(10^{-3}), (\delta X_s)_{rms} \simeq 8(10^{-2}) \ \Delta X$$

it is found that

$$E \simeq 10^{-4}$$

or

$$u_e' \simeq 10^{-4}$$

Hence the overall error in $<\rho' u'>$ is of the order of 1%.

Another perspective on the errors in the calculations is afforded by the quantity $<\rho u>$. For an exact one-dimensional steady shock solution, this quantity should be constant. The results in Table II for the case with no turbulence indicate that the oscillations of the numerical solution can correspond to a jump in $<\rho u>$ of the order of $\pm 3.5 \times 10^{-4}$, depending on where the data are taken. Comparing Figures 14 and 15 showing the correlation $<\rho u>$ for the cases without and with turbulence respectively, it appears that the error in that quantity is nearly the same, independent of the presence of turbulence. The situation is clarified by comparing Figure 14 with Figure 16 which shows the difference between the $<\rho u>$ distribution with turbulence and a shock (Fig. 15) and without a shock as in Figure 17. The fact that the oscillations are of the same order as the observed jump in the turbulent $<\rho' u'>$ raises the question of whether the turbulence is affected by the oscillations. Examining the solutions discussed previously with reference to Figures 5 and 9-13, the oscillations present in the instantaneous pressure distribution (Fig. 5) are much less obvious in the averaged turbulent flow

(Fig. 13). Also, while still present, the numerical oscillations in $<\rho'u'>$ approaching the shock (Fig. 12) are much smaller in amplitude than the change in $<\rho'u'>$ across the shock, and the smoothness of $<\rho'u'>$ indicates that it is not affected significantly by the oscillatory numerical error seen in the $<\rho u>$ and $<\rho><u>$ distributions (Figs. 15 and 18). Thus, it is concluded that the small changes found in the turbulence/shock-wave interaction are due to flow interactions and not to numerical error.

Further confirmation of this conclusion was obtained by calculating the flow on a finer grid with 160 points on each axis. A calculation of 3300 time steps with the turbulence defined at 81 points in the y direction provided the results shown in Figures 19-22. The shock region as defined by the transition from upstream conditions to downstream conditions and exemplified by the mean pressure distribution in Figure 19 is slightly narrower than for the coarser grid. The shock extends from x = 0.0275 to 0.03375, over 11 grid points. Quantitatively, the solutions on the two grids cannot be directly compared, since the turbulence inflow conditions were defined at each point of the inflow boundary in both cases and are therefore different in the two cases. Also, the time step used for the fine grid calculations was half that used for the coarser grid. Thus, the turbulence generated on the fine grid was of a finer scale, both spatially and temporally than that on the coarser grid. However, the solutions for both grids lead to the same conclusion, that the turbulence is affected by the shock wave. The turbulence intensities shown in Figure 20 are of the same order as those in Figure 9. The change in the v' component downstream of the shock is nearly the same in both cases. The u' component, on the other hand, appears to undergo slightly less change for the fine grid. The density and pressure effects also are similar to those on the previous grid. Comparing Figures 21 and 10, the pressure effect is nearly the same on both grids, while the density effect is somewhat less on the fine grid. Turbulence kinetic energy, Figure 22, is slightly decreased on the fine grid from that shown in Figure 11. However, the basic effect of an increase over the no-shock solution is present in both solutions. Finally, the fine grid produces a jump in both the mean p'u' correlation and the mean $\rho'u'$ correlation that is smaller on the fine grid, comparing Figure 23 with Figure 12.

In considering the effects of the shock wave on turbulence which passes through it, the shock wave is generally assumed to be stationary. The factors which are expected to affect the turbulence are, then, the pressure jump, density jump, and velocity jump across the shock. However, it is clear that, except at the side boundaries where the shock location is fixed by the boundary conditions, the shock must move since the shock speed is a function of the upstream flow conditions. Since the conditions upstream of the shock are varying from time-step-to-time-step and point-to-point, the shock speed must vary locally as this nonuniform flow passes through. In addition to this fluctuation of the shock speed, the shape of the shock must also undergo some variance in accordance with the spatial nonuniformity of the flow field. This raises the question of whether the movement and rippling of the shock should be accounted for when calculating the statistics for the turbulence downstream of the shock wave.

Consider the equation for the conservation of mass in a compressible flow

$$\rho_t + (\rho u)_x + (\rho v)_y = 0 \tag{17}$$

where the subscript notation is used to denote partial derivatives. At a normal shock wave, because of the discontinuous flow conditions, the equation for the jump in conditions at the shock becomes

$$[\rho]f_t + [\rho u]f_x + [\rho v]f_y = 0 \tag{18}$$

where the square brackets represent the discontinuous changes in the quantities, and the shock location is given by

$$f(x, y, t) = 0$$

For steady flow, this reduces to

$$[\rho u] = \Delta \tag{19}$$

where Δ is the error in the numerical solution. Dividing Equation (18) by f_x and recognizing that

$$f_t/f_x = -u_s \tag{20}$$

and,

$$f_y/f_x = -(dX_s/dy) \tag{21}$$

the jump condition becomes

$$-[\rho]u_s + [\rho u] - [\rho v(dX_s/dy)] = 0 \tag{22}$$

Let

$$\rho = <\rho> + \rho'$$

$$u = <u> + u'$$

$$v = <v> + v'$$

$$M = dX_s/dy$$

where <> represents the mean value of each quantity, as previously defined. Then Equation 22 becomes, after averaging over the entire solution

$$-[<\rho u_s>] + [<\rho><u> + <\rho' u'>] - [<\rho v M>] = \Delta \tag{23}$$

In order to quantify the shock motion from the results of the numerical calculations, the shock location was assumed to be the point where the local pressure passed through 0.85 with positive gradient. This was a nominal value determined by trial and error to locate a point which was consistently found in the shock capture region.

The change in the turbulence quantity $<\rho' u'>$ across the shock is of the same order as the changes in the shock motion and shock ripple terms as shown in Figures 24 and 25. Both of the shock terms undergo a strong perturbation at the shock and then gradually decline as the correlation between the turbulence and the shock motion decreases with increasing distance from the shock. The reason for the apparent negative correlation between the shock ripple and the ρv product downstream of the shock is not understood at this time. In contrast to this rapidly declining correlation, the $<\rho' u'>$ correlation declines much more slowly after the shock perturbation.

The magnitudes of the shock motion and shock ripple terms are found to be as follows:

$$<u_s'^2>^{1/2} = 0.0556$$

$$<M'^2>^{1/2} = 0.0575$$

Both of these quantities are roughly twice the magnitude of the turbulence intensity terms in the vicinity of the shock shown in Figure 9.

It is recalled that the shock capture region was considered to be a region which could be ignored with respect to the numerical solution, taking only the beginning and end points of the region as accurate. Confirmation of this assessment is offered by Figure 26 wherein is shown the net mass flux as given by

$$<N> = - <\rho u_s> + <\rho u> - <\rho v M> \qquad (24)$$

The beginning and end of the shock region are at approximately x = 0.0275 and 0.035 respectively, as discussed previously. The value of the balance is nearly the same at the two points, even though the balance changes significantly between the points. Thus, the mass balance after the shock is nearly the same as it was ahead

of the shock. This is as it should be, allowing for some entrainment of fluid due to the fact that the region for which the statistics are calculated is not bounded by solid walls.

In the interest of turbulence modeling, the effects of the shock wave on the turbulence kinetic energy is of great importance. The quantity presented in Figures 11 and 22 is the kinetic energy of the turbulence fluctuations,

$$\langle k \rangle = (\langle \rho u'u' \rangle + \langle \rho v'v' \rangle)/2 \tag{25}$$

This quantity contains the density and its fluctuations as well as the velocity fluctuations of the turbulent flow. It is important to determine whether the increase in this quantity downstream of the shock observed in Figures 11 and 22 is due to factors in addition to the 25-percent increase in density across the shock jump. For this purpose, it is more instructive to examine a quantity which contains only turbulence quantities. For turbulence models, the quantity of most interest in the present context would be

$$k^* = (\langle u'u' \rangle + \langle v'v' \rangle)/2 \tag{26}$$

The variation of $\langle u'u' \rangle$ and $\langle v'v' \rangle$ and of k^* are shown in Figures 27 and 28, respectively. The $\langle u'u' \rangle$ and $\langle v'v' \rangle$ exhibit the same kind of behavior as the $\langle u'u' \rangle^{1/2}$ and $\langle v'v' \rangle^{1/2}$ of Figure 9. Similarly, the k^* variation indicates an increase over the no-shock case of approximately 30-percent. It is also observed in Figures 9 and 27 and 11 and 28 that the decay rate of the various quantities is changed significantly immediately downstream of the shock, increasing slightly for $\langle v'v' \rangle$ and decreasing greatly for $\langle u'u' \rangle$. This condition exists only for a short distance downstream of the shock where the decay rate resumes a trend nearly parallel to the no-shock case. Thus, the kinetic energy of the turbulence is increased over the no-shock case through an increase in the intensity of the velocity fluctuations through the shock, and then becomes further displaced from the no-shock case through the apparent decrease in the dissipation and remains at a higher level than for the no-shock case as the decay returns to the unshocked rate.

If an analysis like that discussed previously with respect to the conservation of mass is performed for the conservation of momentum and the equation for the transport of turbulence kinetic energy, it is clear that terms containing the shock motion and shock ripple will appear. It has been demonstrated that the shock motion and ripple produce terms of the same order as the density-velocity correlations and turbulence intensity of the flow field. While an exact cause-and-effect relationship has not yet been established, it is strongly suggested by these observations that the shock motion may be a significant factor in the production of turbulence kinetic energy by the shock. An analysis relating the increase in turbulence kinetic energy to the shock motion is presented in Appendix A.

Finally, the shock wave/turbulence interaction is observed to produce a net increase in the streamwise mass flux within the channel defined by the turbulent inflow. In Figure 17, the mass flux in that channel was shown for the case with no shock wave. The mass flux increases slightly in the streamwise direction. Recalling Figure 16, where the difference in the mass flux between the shocked and non-shocked case is shown, the difference upstream of the shock is essentially zero, except for the oscillations which increase as the shock is approached and then decrease as the shock is passed. After the shock, as the oscillations diminish, the difference shows an increasing trend.

The observations discussed herein lead to the conclusion that there is a correlation between the fluctuating density in the vicinity of the shock and the fluctuating local shock speed, and that the simple jump relation that exists for the unperturbed mean flow, namely $\rho_1 u_1 = \rho_2 u_2$ does not carry over to the turbulent flow. In fact, it is found that the correlation between ρ' and u_s is of the same order as for ρ' and u'. Furthermore, the magnitude of the rms fluctuation in u_s and in dX_s/dy are both of the same order as the turbulence intensity components. A similar analysis may be constructed for the momentum and energy equations. This suggests that an important ingredient of a model of turbulence interacting with a shock is the coupling between the shock motion and the density, energy, and velocity fields.

INDICIAL ANALYSIS

In unsteady transonic aerodynamics, it is observed that the shock motion is nearly linearly dependent on the unsteady forcing function and, because of this linearity, an "indicial" formulation of the shock motion as proposed by Nixon (Ref. 5) can be used. In such a formulation the shock location for any time-dependent forcing function is related to its "indicial response" to a step change in the forcing function through a convolution integral. Thus, if $\delta X_s(t)$ is the shock location, then

$$\delta X_s(t) = \delta X_{s_\epsilon}(t)\epsilon(0) + {}_0\int^t \delta X_{s_\epsilon}(\tau)\frac{d\epsilon(t-\tau)}{dt}\, d\tau \tag{27}$$

where $\delta X_{s\epsilon}(t)$ is the transient response to a unit step change in some parameter ϵ; $\epsilon(t)$ is an arbitrary schedule of the parameter ϵ, and $\delta X_s(t)$ is then the shock location due to this schedule. In view of the power of this theory in unsteady transonic flow, it was decided to investigate its applicability to turbulence. That is, the parameter ϵ is taken to be the independent subset of the turbulence quantities u', v', ρ', and p'; at this stage the correct subset has not been determined. The validation of this indicial function idea is discussed in Appendix B.

In the indicial analysis for transonic flow it is frequently convenient to represent the numerically generated indicial response function, $\delta X_{s\epsilon}(t)$, by a simple series, such as

$$\delta X_{s_\epsilon}{}^{(n)}(t) = \frac{\delta X_s{}^{(n)}(\infty)}{\epsilon_o{}^{(n)}} \left[1 - \exp(-a^{(n)}t)\right] \left[1 + \sum_{l=1}^{N} b_l{}^{(n)} \exp(-a_n{}^{(n)}lt)\right] \tag{28}$$

where $\delta X_{s\epsilon}{}^{(n)}$ is the indicial response due to a step change in the variable $\epsilon^{(n)}$ of $\epsilon_o{}^{(n)}$, $\delta X_s{}^{(n)}(\infty)$ is the value of $\delta X_s(t)$ as $t \to \infty$ and $a^{(n)}$ and $b_l{}^{(n)}$ are constants associated with the variable $\epsilon^{(n)}$.

Consider now the response of the shock wave to the nth turbulence quantity $f^{(n)}(x_j,t)$ where x_j is the spatial vector and t is time. $f(x_j,t)$ may be expanded as a Fourier series to give

$$f^{(n)}(x_j,t) = \sum_{m=-\infty}^{\infty} \bar{f}_m^{(n)}(x_j)\exp(i\omega mt) \tag{29}$$

where ω is some fundamental frequency and $\bar{f}_m^{(n)}(x_j)$ is a function of x_j

If $f^{(n)}(x_j,t)$ is identified with ϵ in Equation (27), and if the frequencies of turbulence are high, then using the result obtained in Reference 5, it may be shown that

$$\delta X_s^{(n)}(x_j,t) \simeq \frac{\delta X_s^{(n)}(\infty)}{\epsilon_o^{(n)}} \frac{a^{(n)}}{\omega}\left[1 + \sum_{l=1}^{N} b_l^{(n)}\right] x \sum_{m=-\infty}^{\infty} f_m^{(n)}(x_j) \frac{\exp(i\omega mt - i\pi/2)}{m} \tag{30}$$

or,

$$\delta X_s^{(n)}(x_j,t) = -\frac{-i\delta X_s^{(n)}(\infty)a^{(n)}}{\epsilon_o^{(n)}}\left[1 + \sum_{l=1}^{N} b_l^{(n)}\right]\left[\int^t f^{(n)}(x_j,\tau)d\tau - 1\right]\exp(-i\pi/2) \tag{31}$$

Differentiation with respect to time gives after some rearrangement

$$\frac{d\delta X_s^{(n)}(t)}{dt} = u_s^{(n)}(t) = \frac{-i\delta X_s^{(n)}(\infty)a^{(n)}}{\epsilon_o^{(n)}}\left[1 + \sum_{l=1}^{N} b_l^{(n)}\right] f^{(n)}(x_j,t)\exp(-i\pi/2) \tag{32}$$

and thus the shock speed becomes a linear combination of the turbulence variables $f^{(n)}(x_j,t)$. It can also be seen from Equation (30) that if the frequency, ω, of the turbulence tends to infinity, the shock location does not change but the shock speed has a magnitude of the same order as the turbulence quantities.

It is of interest to consider the spatial derivative of $\delta X_s^{(n)}(\infty)$. Differentiation of Equation (31) with respect to x_j gives

$$M^{(n)}(x_j,t) = \frac{\partial \delta X_s^{(n)}}{\partial x_j} = \frac{-i\delta X_s^{(n)}(\infty) a^{(n)}}{\epsilon_o^{(n)}} \left[1 + \sum_{l=1}^{N} b_l^{(n)} \right] \left[\int^t \frac{\partial f^{(n)}}{\partial x_j} d\tau \right] \exp(-i\pi/2) \tag{33}$$

If $\partial f^{(n)}/\partial x_j$ is the same order of magnitude as $\partial f^{(n)}/\partial t$ then the shock ripple, $M^{(n)}(x_j,t)$, has the same order of magnitude as the shock speed, $u_s^{(n)}(x_j,t)$ and, hence, also as the turbulence quantities.

In this analysis, the constants $a^{(n)}$, $b^{(n)}$, and $\delta X^{(n)}(\infty)/\epsilon_o^{(n)}$ may be dependent on the geometry of the problem, a result inferred from work in transonic aerodynamics. Hence, the relation between the shock speed and ripple and the turbulence quantities may not be universal.

The analysis in this section implies the following relations.

(a). The shock speed is the same order of magnitude as the turbulence quantities and is a linear combination of them.

(b). The shock ripple may be of the same order of magnitude as the shock speed.

(c). The shock motion is an order of magnitude smaller than the shock speed.

CONCLUSIONS AND RECOMMENDATIONS

The work reported herein represents the first step in a study of shock waves interacting with turbulence. The overall goals of the study are to determine the mutual effects of the interaction and to determine improvements for turbulence models in the presence of shock waves. The ultimate goal is to extend this knowledge to improving turbulence models in the presence of shock waves at hypersonic speeds.

Two short term goals for the present study were to develop an accurate numerical approach in two dimensions which would serve to illuminate the problems that may be encountered in the long range study and to aid in determining methods of analyzing the turbulence. These goals were accomplished by developing a computer code employing MacCormack's explicit numerical method to solve the Navier-Stokes equations for a normal shock wave encountering turbulence.

Another short term goal was to develop insight into shock/turbulence interaction. This was accomplished by employing a low supersonic Mach number which allowed the study to take place in an environment for which the basic elements of the flow are well understood, and also to make use of certain expedients available from transonic flow theory. The major insight that was obtained from the work was that shock/turbulence interaction contains influences from the shock motion that are quite unapparent from a Reynolds averaged point of view. This conclusion must be examined further using three-dimensional turbulence and higher Mach numbers. Also, the work must be extended to encompass oblique shocks interacting with turbulence in a shear flow, since such are the flows that will ultimately be of most interest.

Another short term goal of the work was to extend the numerical approach to three dimensions. The effort to date has centered on developing the appropriate analytical and computational tools for the analysis of turbulence/shock wave interactions. The computer code used in these preliminary calculations has been combined with another code employing the same algorithm already possessing the required three-dimensional capability. The turbulence statistics, boundary condition

treatment, and turbulence generation used in the two-dimensional code have thus been extended to three dimensions. The code is now ready for a fully three-dimensional treatment of the turbulence.

Examination of the solutions generated by the two-dimensional code indicated that the numerical errors that are inherent in the explicit MacCormack algorithm do not affect the turbulence calculations. Large oscillations are produced by discontinuous changes in the mean flow quantities, but the perturbation quantities undergo smaller changes and change more smoothly. Therefore, the pertubation quantities exhibit only relatively small oscillations. Thus, the turbulence calculations are believed to be accurate to within the truncation error for the numerical method.

Several observations were made which indicate the shock has a significant effect on the turbulence. The shock produces a jump in the turbulence quantities, with a long relaxation distance to return to unshocked values. The turbulence kinetic energy is increased by 30 percent by the shock. The density-velocity correlation, $<\rho' u'>$, becomes important during the shock jump and is greatly increased over the case without a shock. On the other hand, the pressure-velocity correlation, $<p' u'>$, is not quite so important.

Using the no-shock case as a guide, the rate of decay before and after the shock indicates that the dissipation, ϵ, changes only slightly compared to the kinetic energy. Thus, if eddy viscosity is defined as $\nu_t \simeq k^2/\epsilon$, the ratio of ν_t before and after the shock is $k_1^2/k_2^2 \simeq 2$. This has implications regarding heat transfer which can change dramatically because of changes in ν_t.

The results show that shock speed and ripple may be important factors in determining the turbulence downstream of a shock wave. Shock speed and ripple correlations are the same size as other important turbulence correlations, such as, $<\rho' u'>$, $<u' u'>$, $<p' u'>$, and k; shock ripple terms may be more important for oblique shocks because of larger v component.

Transonic indicial theory applied to the shock/turbulence interaction leads to several interesting observations. For example, while undergoing fluctuations in velocity equal to the turbulent velocity fluctuations of the flow field, the shock

location moves only slightly. Another observation is that shock speed correlations are a linear combination of correlations of turbulent flow quantities. Jump correlations for shock speed are about the same order of magnitude as the flow correlation jumps.

In conclusion, this work has demonstrated that there are potentially very important interactions between a shock wave and a turbulent flow field. The approach taken, employing available numerical computational tools and an approximate representation of turbulence, has provided useful insights for expanding the research to encompass more realistic flow configurations and conditions. While two-dimensional turbulence is not realistic, for the purposes outlined in this report it contains the essential elements of a fluctuating flow field. It is strongly recommended that future calculations be done in a three-dimensional turbulence field. Also, a larger computational domain is needed to check the relaxation distance of the shock effects on the turbulence and to isolate the computation from boundary effects. A more accurate algorithm is needed in order to eliminate any question of the effect of the numerical errors on the observed turbulence after the shock. Finally, calculations should be done for an oblique shock in order to obtain stronger v correlations.

REFERENCES

1. Shang, J. and Hankey, W. L.: Numerical Solution for Supersonic Turbulent Flow over a Compression Ramp, AIAA Journal, Vol. 13, No. 10, October 1975, pp. 1368-1374.

2. Hinze, J. O.: Turbulence, Second Edition, McGraw-Hill, Inc., New York, 1975.

3. Rogallo, R. S. and Moin, P.: Numerical Simulation of Turbulent Flows, Annual Review of Fluid Mechanics, Vol. 16, 1984, p. 120.

4. Nixon, D.: Behavior of the Flow Through a Numerically Captured Shock Wave, AIAA Journal, Vol. 22, No. 1, January 1984, pp. 150-151.

5. Nixon, D.: Notes on the Indicial Method, AIAA Journal, Vol. 16, No. 6, June 1978, pp. 613-616.

Table I.

List of rms values of u', v', ρ', and p' for steady shock case.

X	u'rms	v'rms	ρ'rms	p'rms
0.00000	7.12319E-06	1.44329E-06	7.39986E-06	7.03310E-06
0.00125	2.44887E-06	0.00000E+00	5.96046E-08	1.04606E-06
0.00250	7.20255E-06	1.44321E-06	7.37847E-06	7.02020E-06
0.00375	3.31865E-06	7.10731E-08	3.00102E-06	2.51402E-06
0.00500	8.46386E-06	2.27635E-06	8.73325E-06	8.37122E-06
0.00625	5.46286E-06	4.38622E-07	5.15468E-06	5.04989E-06
0.00750	1.04541E-05	3.45727E-06	1.07116E-05	1.03719E-05
0.00875	8.53908E-06	1.38007E-06	8.41271E-06	8.31928E-06
0.01000	1.31752E-05	5.23048E-06	1.34059E-05	1.31232E-05
0.01125	1.26839E-05	3.21078E-06	1.27408E-05	1.26148E-05
0.01250	1.75992E-05	7.98542E-06	1.79207E-05	1.75934E-05
0.01375	1.91810E-05	6.38178E-06	1.95491E-05	1.93972E-05
0.01500	2.51577E-05	1.20906E-05	2.58342E-05	2.54843E-05
0.01625	2.88457E-05	1.10556E-05	2.97493E-05	2.95925E-05
0.01750	3.50163E-05	1.69789E-05	3.62608E-05	3.59802E-05
0.01875	3.80046E-05	1.54531E-05	3.94589E-05	3.94713E-05
0.02000	4.06055E-05	1.92527E-05	4.20449E-05	4.20517E-05
0.02125	3.80670E-05	1.47329E-05	3.92283E-05	3.95789E-05
0.02250	3.49481E-05	1.47206E-05	3.55554E-05	3.57724E-05
0.02375	2.90470E-05	7.81580E-06	2.92946E-05	2.96241E-05
0.02500	3.08264E-05	8.70620E-06	3.08959E-05	3.08293E-05
0.02625	2.90521E-05	4.04505E-06	2.96802E-05	2.95422E-05
0.02750	5.16982E-05	8.59280E-06	5.07960E-05	5.16102E-05
0.02875	7.75456E-06	1.03651E-06	1.24250E-05	9.88898E-06
0.03000	2.23273E-04	1.13871E-05	2.26297E-04	2.37557E-04
0.03125	1.61209E-04	4.52128E-05	1.95533E-04	2.04737E-04
0.03250	3.78583E-05	3.66188E-05	3.83401E-05	4.57391E-05
0.03375	1.80216E-05	3.88444E-05	1.92622E-05	2.06197E-05
0.03500	5.37351E-05	2.77664E-05	6.09432E-05	6.77737E-05
0.03625	2.63460E-05	2.20543E-05	2.66304E-05	2.92868E-05
0.03750	4.46592E-05	1.36363E-05	5.04349E-05	5.59164E-05
0.03875	2.65819E-05	7.22448E-06	2.80054E-05	3.07446E-05
0.04000	3.18990E-05	3.29671E-06	3.63368E-05	4.03315E-05
0.04125	2.05268E-05	6.16266E-06	2.25863E-05	2.47881E-05
0.04250	1.94939E-05	7.88442E-06	2.26921E-05	2.53252E-05
0.04375	1.57339E-05	1.13655E-05	1.90377E-05	2.09183E-05
0.04500	1.16217E-05	1.17925E-05	1.37166E-05	1.53833E-05
0.04625	1.52566E-05	1.35844E-05	1.98255E-05	2.18449E-05
0.04750	1.01664E-05	1.30935E-05	1.12954E-05	1.24460E-05
0.04875	1.47201E-05	1.37006E-05	1.95935E-05	2.16414E-05

Table II.

List of $\langle u \rangle$, $\langle v \rangle$, $\langle \rho \rangle$, $\langle p \rangle$, and $\langle \rho u \rangle$ for steady shock case.

Theoretical Values at shock jump:

u_1	= 1.15	u_2	= 0.916305
ρ_1	= 1.0	ρ_2	= 1.25504
v_1	= 0.0	v_2	= 0.0
p_1	= 0.714286	p_2	= 0.98286
$\langle \rho u \rangle_1$	= 1.15	$\langle \rho u \rangle_2$	= 1.15

X	$\langle u \rangle$	$\langle v \rangle$	$\langle \rho \rangle$	$\langle p \rangle$	$\langle \rho u \rangle$
0.00000	1.150027	6.07867E-08	0.999971	0.714258	1.14999
0.00125	1.150000	0.00000E+00	1.000000	0.714286	1.15000
0.00250	1.149972	-6.07837E-08	1.000029	0.714314	1.15001
0.00375	1.150010	1.02647E-11	0.999991	0.714276	1.15000
0.00500	1.149964	-9.57456E-08	1.000037	0.714322	1.15001
0.00625	1.150024	1.39344E-08	0.999977	0.714262	1.15000
0.00750	1.149947	-1.45508E-07	1.000054	0.714339	1.15001
0.00875	1.150047	5.19740E-08	0.999953	0.714238	1.14999
0.01000	1.149919	-2.23606E-07	1.000083	0.714367	1.15001
0.01125	1.150086	1.35955E-07	0.999913	0.714199	1.14999
0.01250	1.149871	-3.62275E-07	1.000132	0.714415	1.15002
0.01375	1.150150	3.14396E-07	0.999848	0.714134	1.14999
0.01500	1.149790	-6.27321E-07	1.000214	0.714497	1.15004
0.01625	1.150258	6.64969E-07	0.999738	0.714026	1.14996
0.01750	1.149652	-1.07788E-06	1.000355	0.714636	1.15006
0.01875	1.150439	1.16248E-06	0.999554	0.713844	1.14993
0.02000	1.149418	-1.51634E-06	1.000592	0.714871	1.15010
0.02125	1.150735	1.36886E-06	0.999252	0.713545	1.14987
0.02250	1.149020	-1.35362E-06	1.000995	0.715272	1.15016
0.02375	1.151165	8.29798E-07	0.998808	0.713109	1.14979
0.02500	1.148177	-6.89811E-07	1.001815	0.716110	1.15026
0.02625	1.151036	3.19065E-07	0.998812	0.713187	1.14967
0.02750	1.143497	-5.40899E-07	1.006029	0.720638	1.15039
0.02875	1.137744	1.03004E-07	1.010291	0.725830	1.14945
0.03000	1.084217	-7.05174E-07	1.061083	0.780058	1.15044
0.03125	0.961642	-2.69602E-06	1.195909	0.922350	1.15004
0.03250	0.924830	-2.22471E-06	1.243277	0.971103	1.14982
0.03375	0.918577	-2.15126E-06	1.251994	0.979883	1.15005
0.03500	0.916195	-1.53559E-06	1.255089	0.983130	1.14991
0.03625	0.916602	-9.97246E-07	1.254663	0.982625	1.15003
0.03750	0.915980	-5.79323E-07	1.255409	0.983443	1.14993
0.03875	0.916406	-5.55969E-08	1.254908	0.982887	1.15000
0.04000	0.916056	1.42036E-07	1.255322	0.983344	1.14995
0.04125	0.916332	4.97701E-07	1.254997	0.982985	1.14999
0.04250	0.916121	5.41513E-07	1.255247	0.983261	1.14996
0.04375	0.916295	7.36329E-07	1.255042	0.983035	1.14999
0.04500	0.916169	6.99422E-07	1.255191	0.983200	1.14997
0.04625	0.916278	7.83975E-07	1.255063	0.983058	1.14999
0.04750	0.916205	7.14981E-07	1.255150	0.983155	1.14998
0.04875	0.916273	7.35186E-07	1.255071	0.983067	1.14999

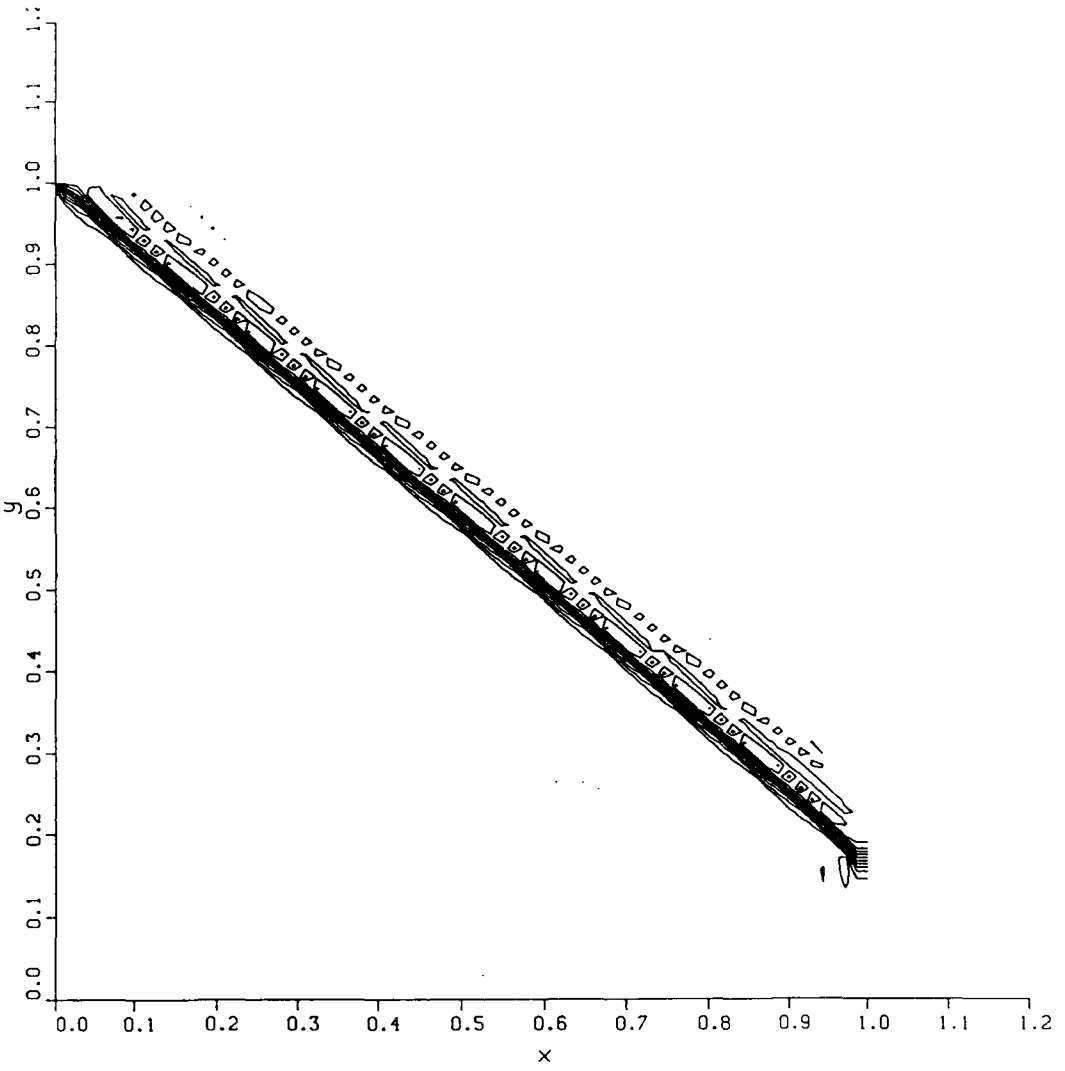

a. Contours of constant density from code 1 (Ref. 1).

Figure 1. Comparison of Navier-Stokes solvers.

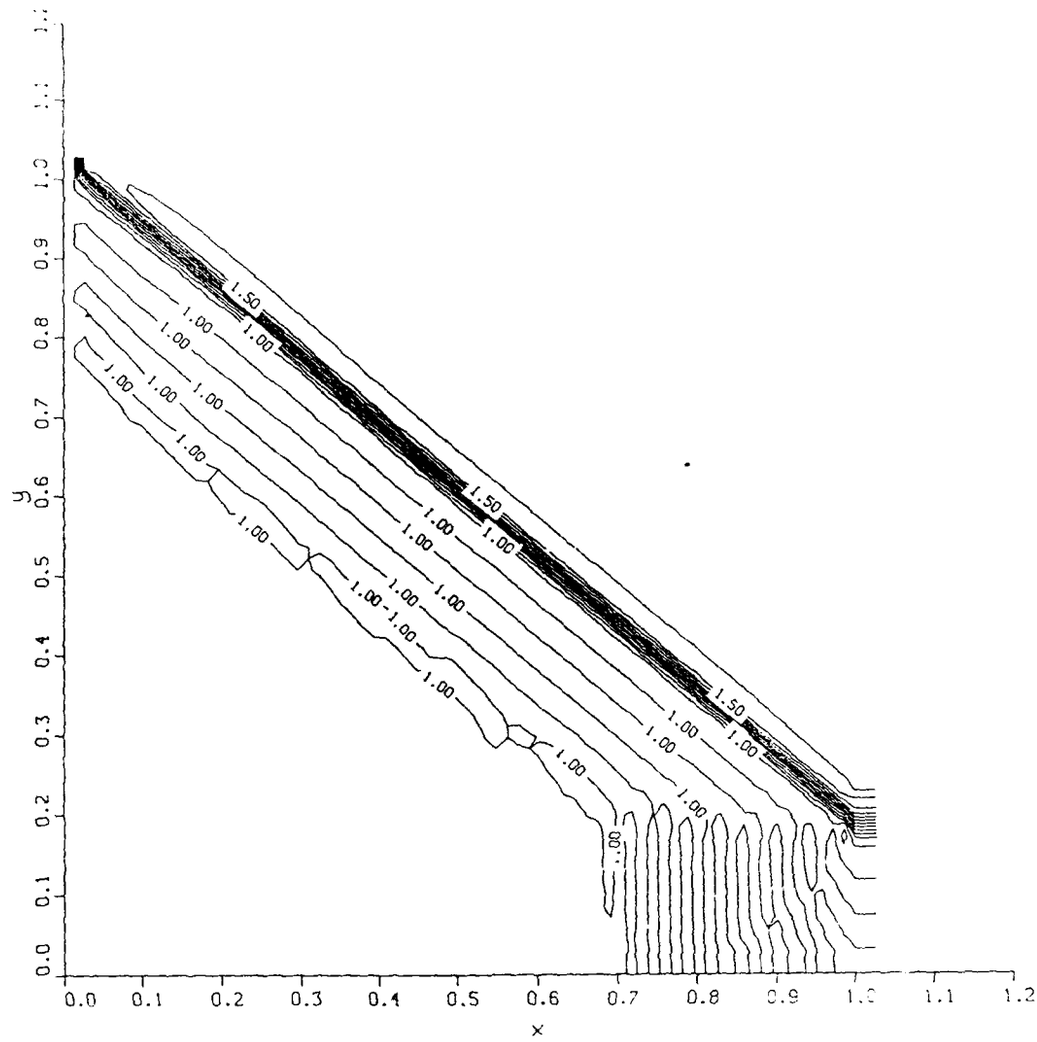

b. Contours of constant density from code 2 (Present work).

Figure 1. Continued

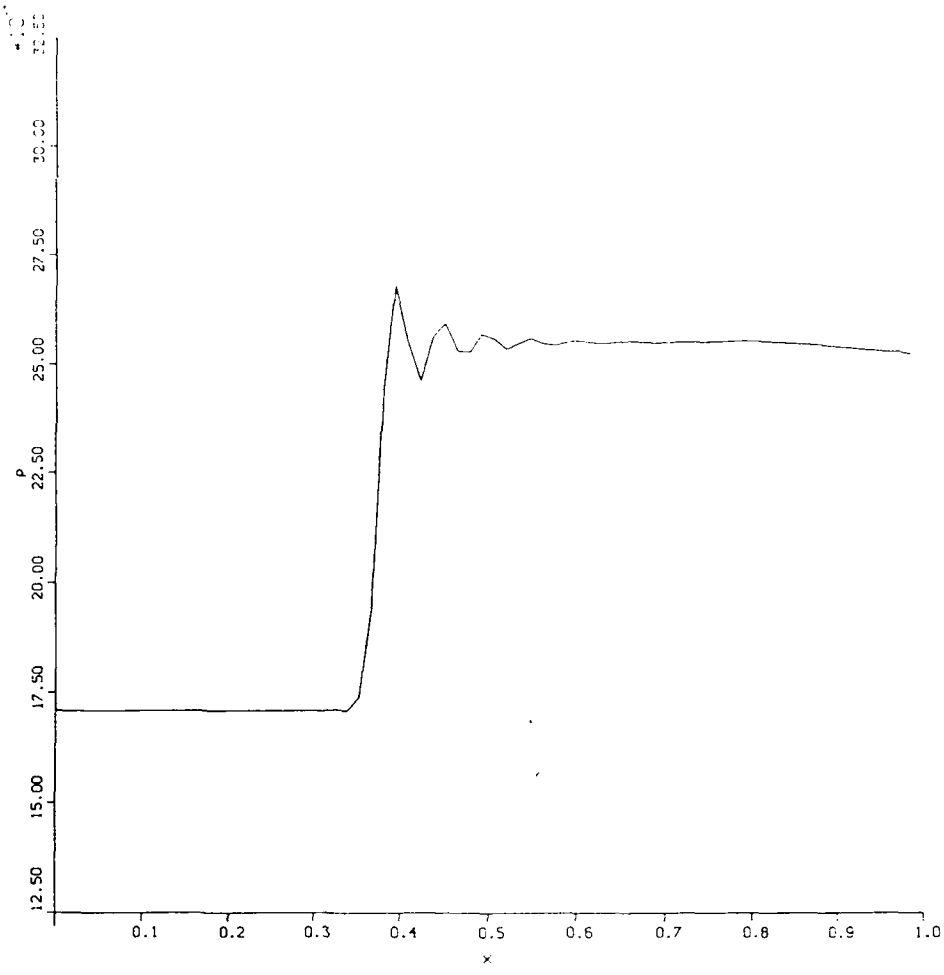

c. Density variation through shock wave from code 1.

Figure 1. Continued

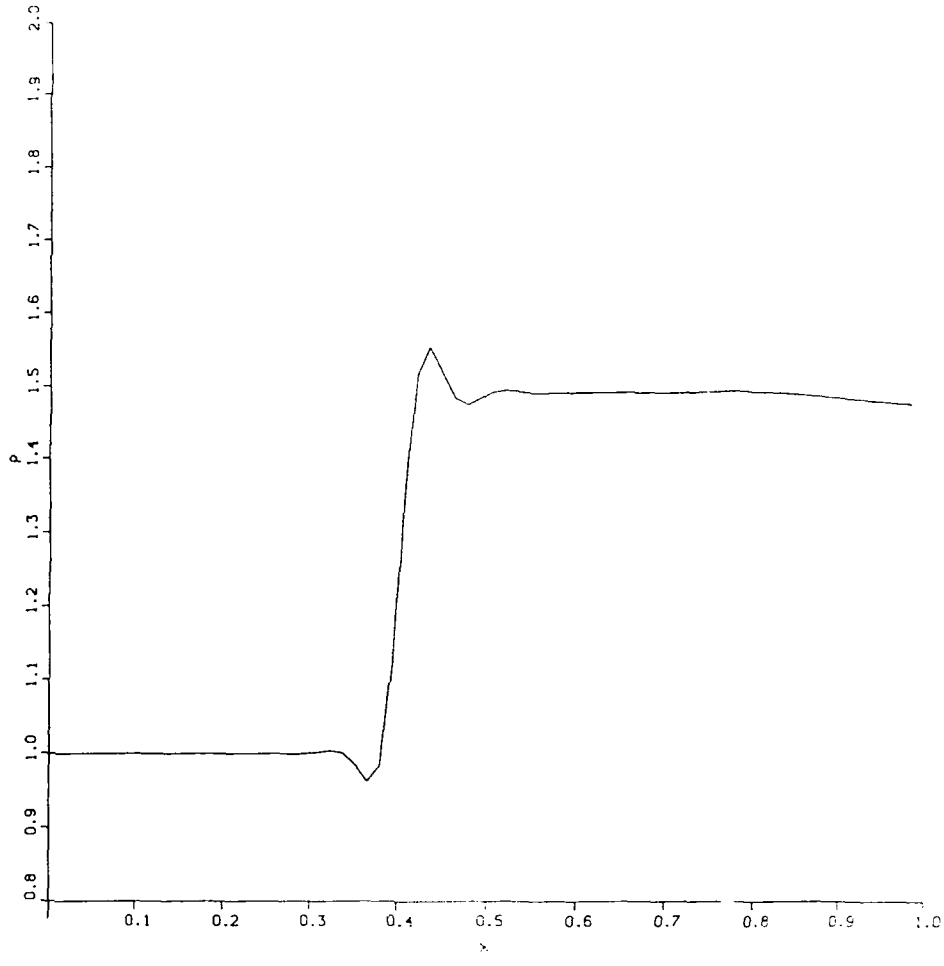

d. Density variation through shock wave from code 2.

Figure 1. Concluded

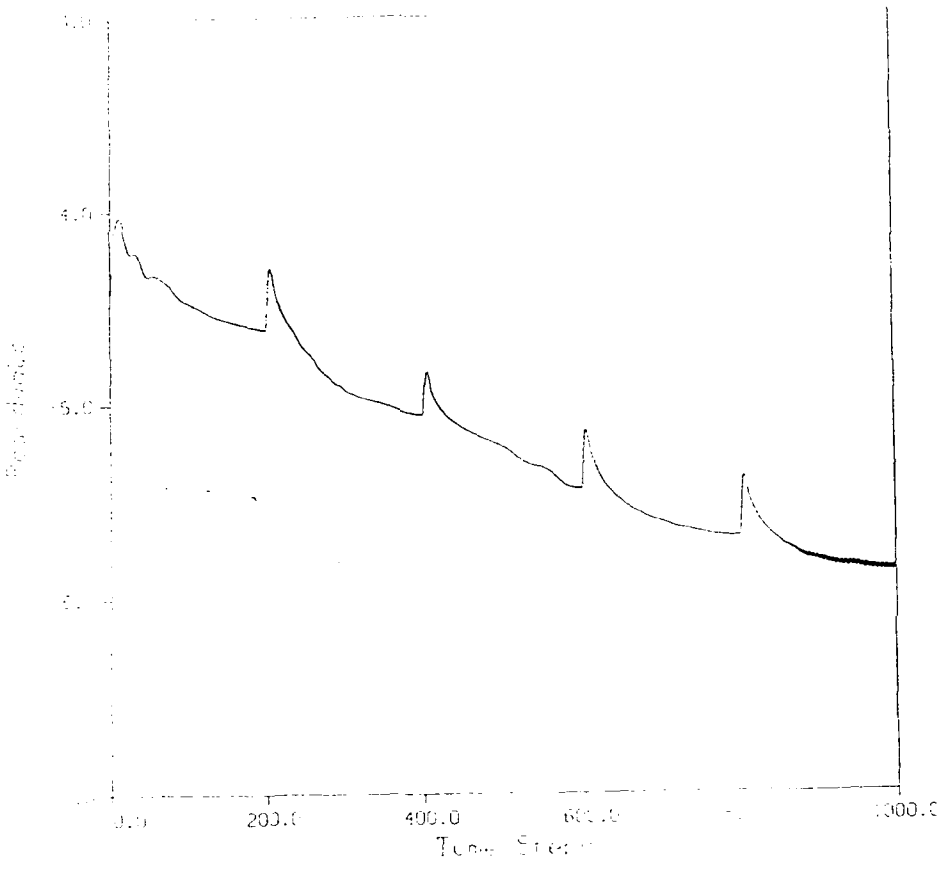

Figure 2. Convergence history of maximum error.

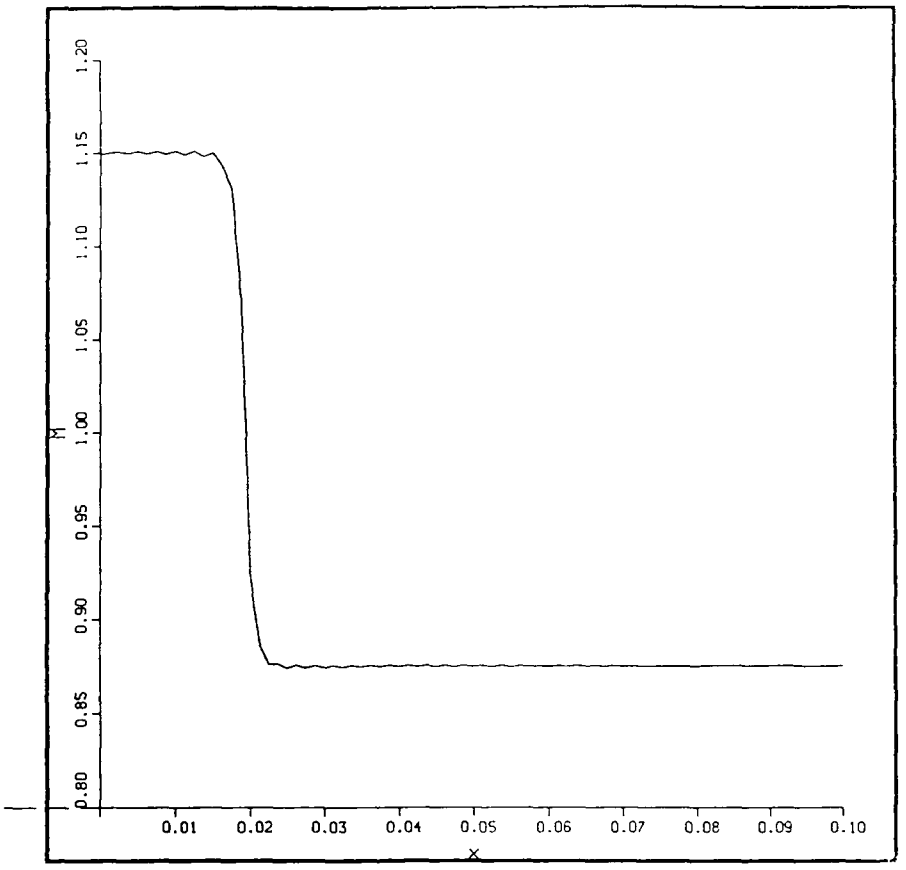

a. Re = 10000; No artificial dissipation.

Figure 3. Dissipation and Reynolds number effects on calculated Mach number through the shock wave.

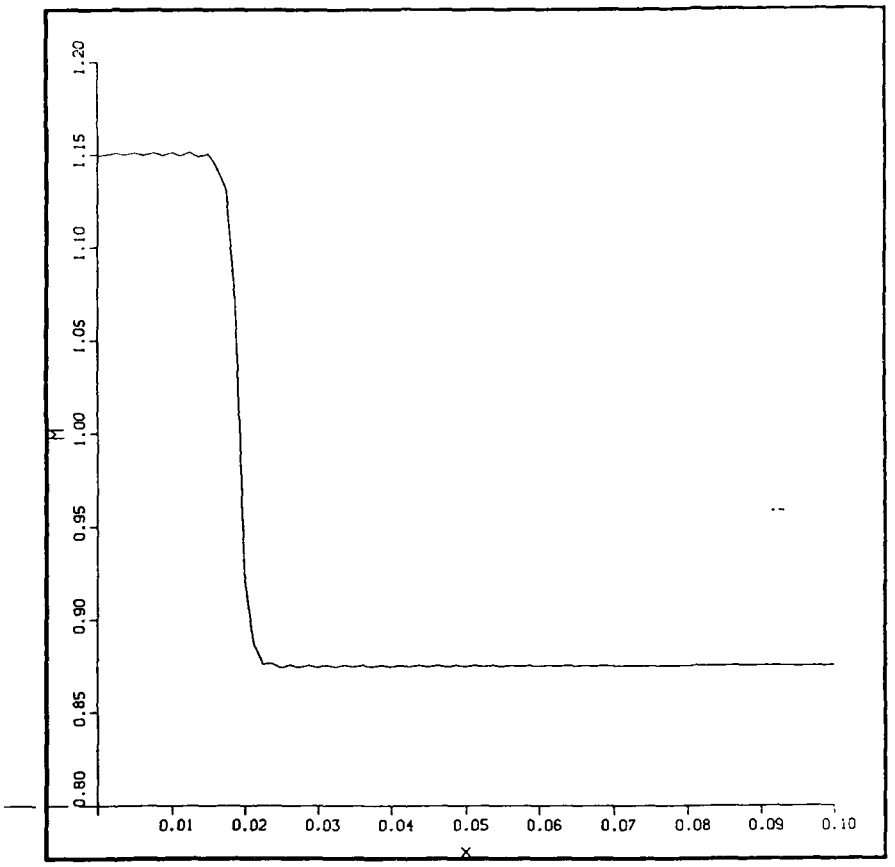

b. Re = 10000; Second order artificial dissipation.

Figure 3. Continued

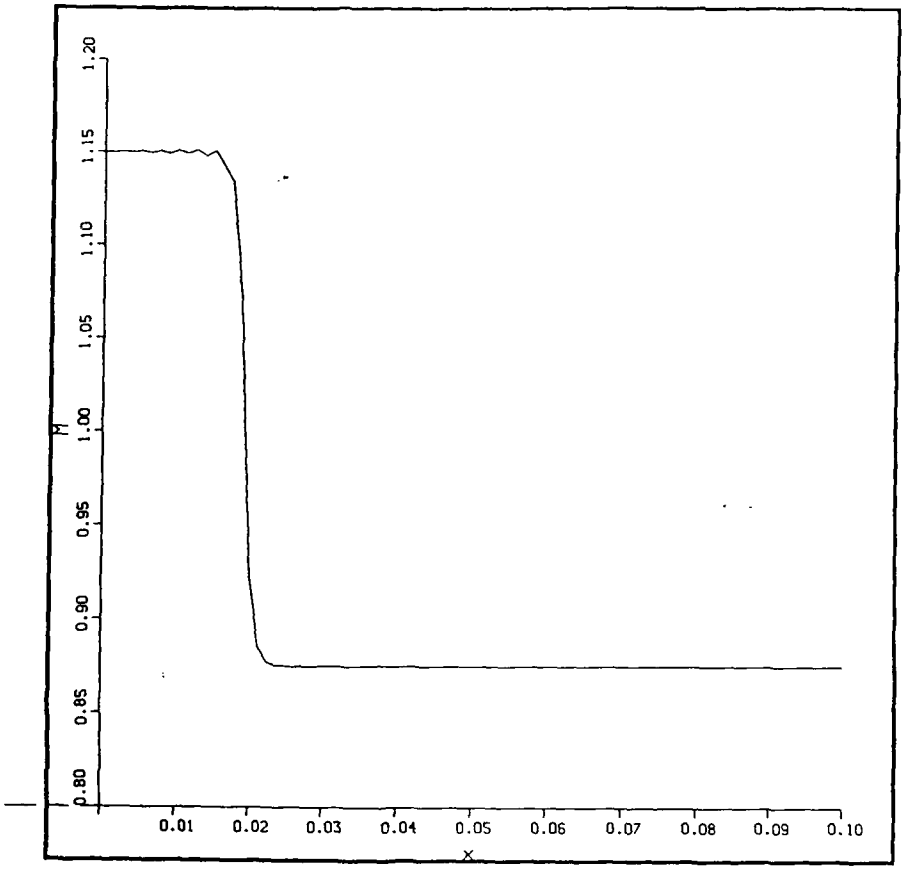

c. Re = 10000; Fourth order artificial dissipation.

Figure 3. Continued

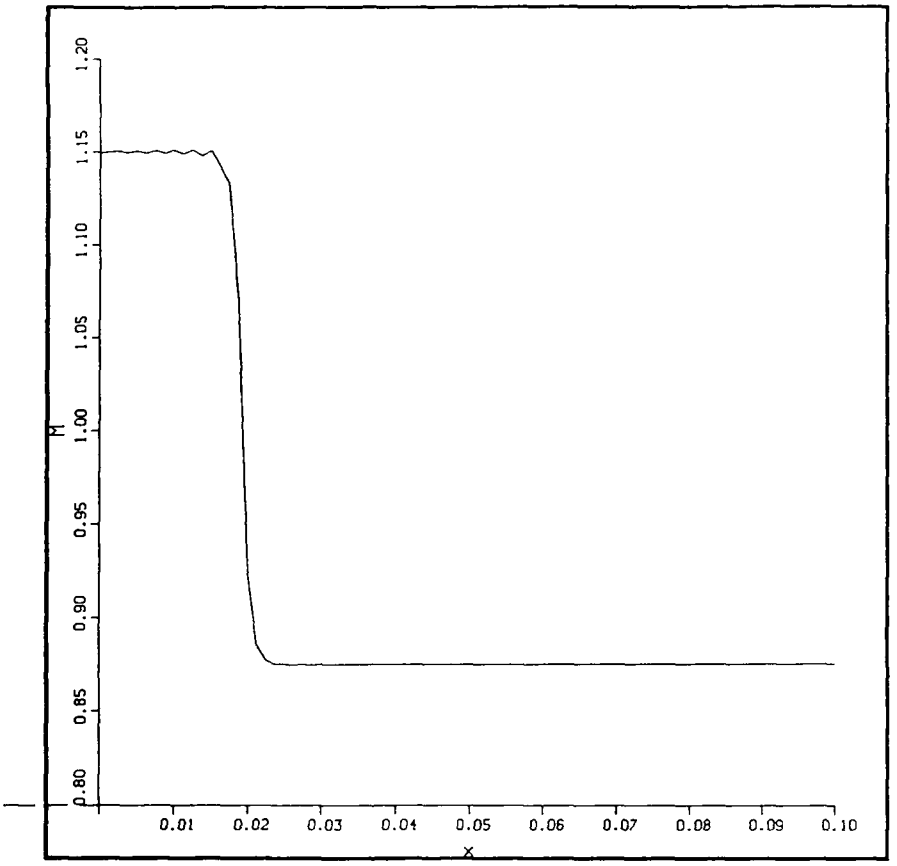

d. Re = 10000; Second and fourth order artificial dissipation.

Figure 3. Continued

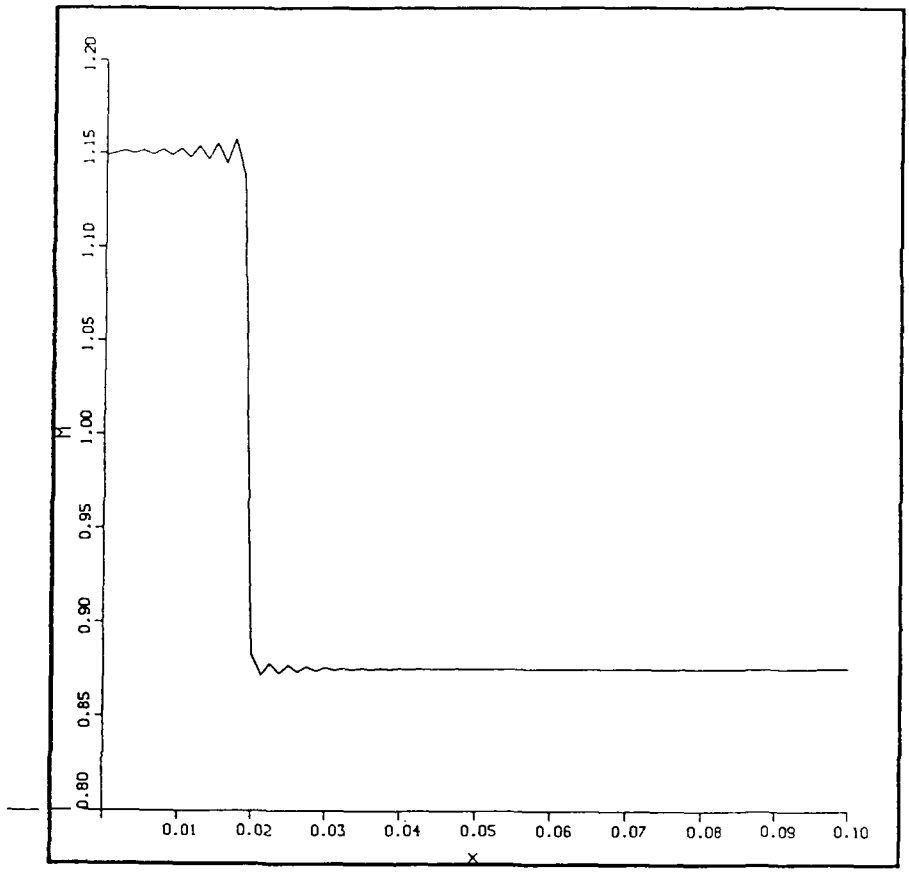

e. Re = 100000; Second and fourth order artificial dissipation.

Figure 3. Continued

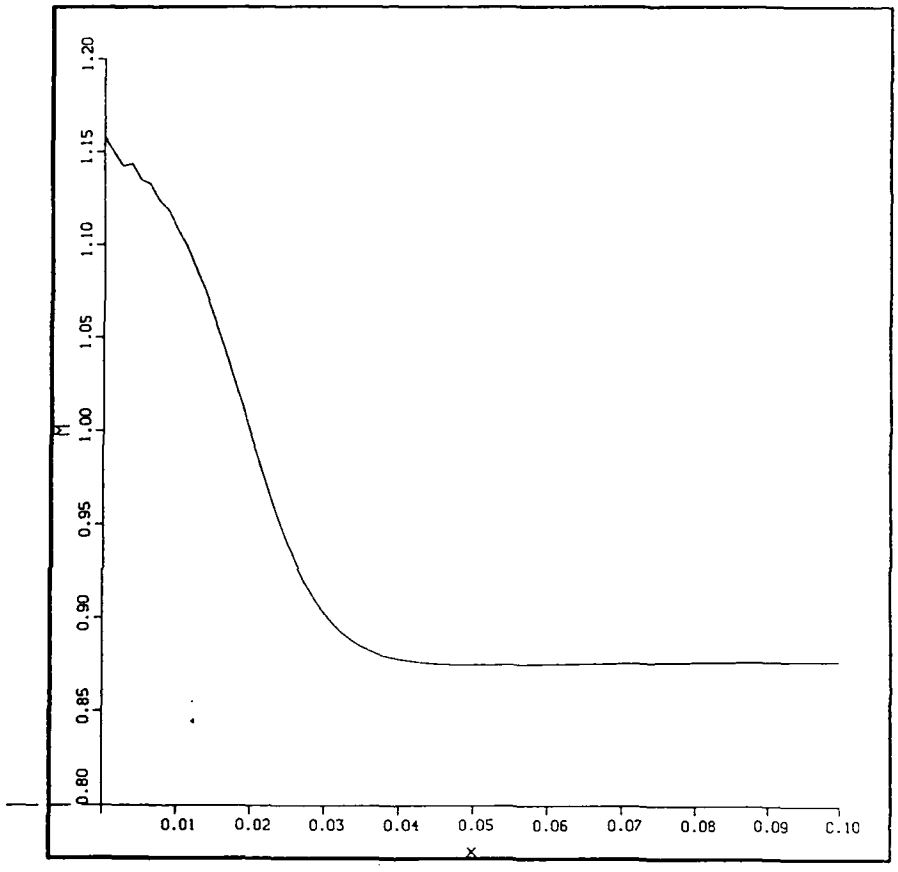

f. Re = 1000; Second and fourth order artificial dissipation.

Figure 3. Concluded

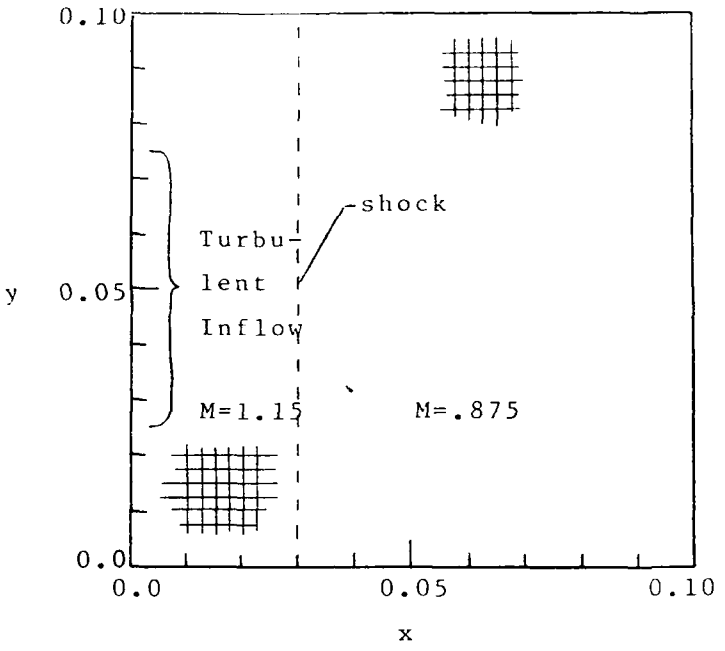

Figure 4. Computational space.

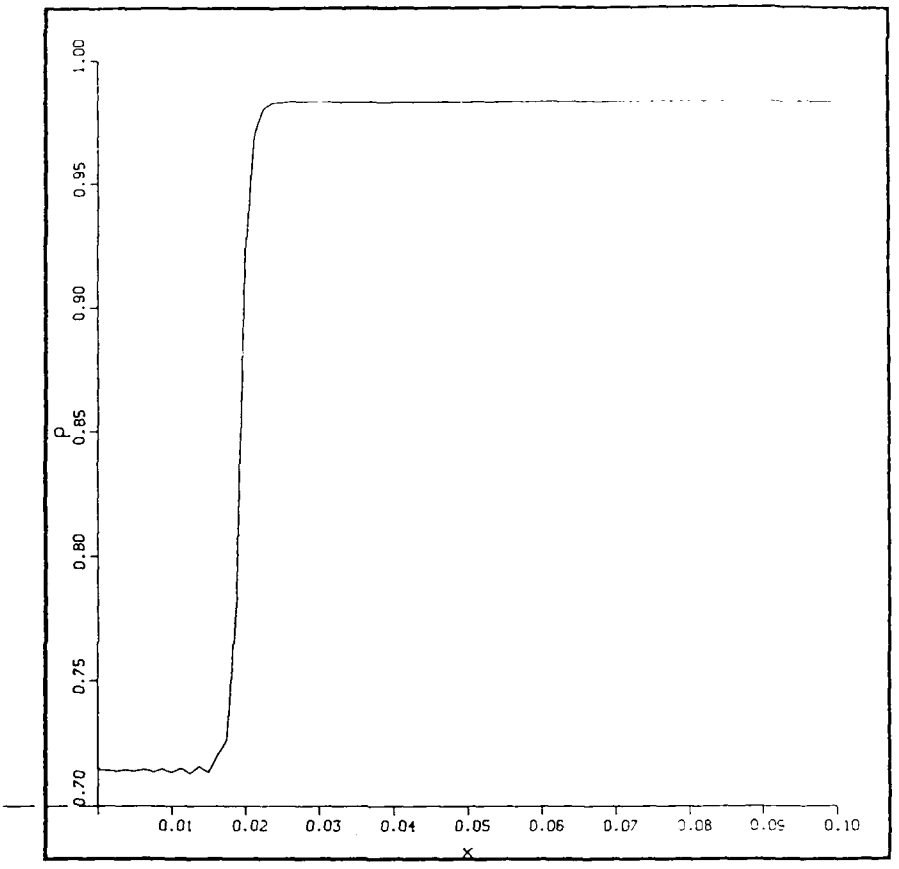

Figure 5. Steady pressure distribution through the shock.

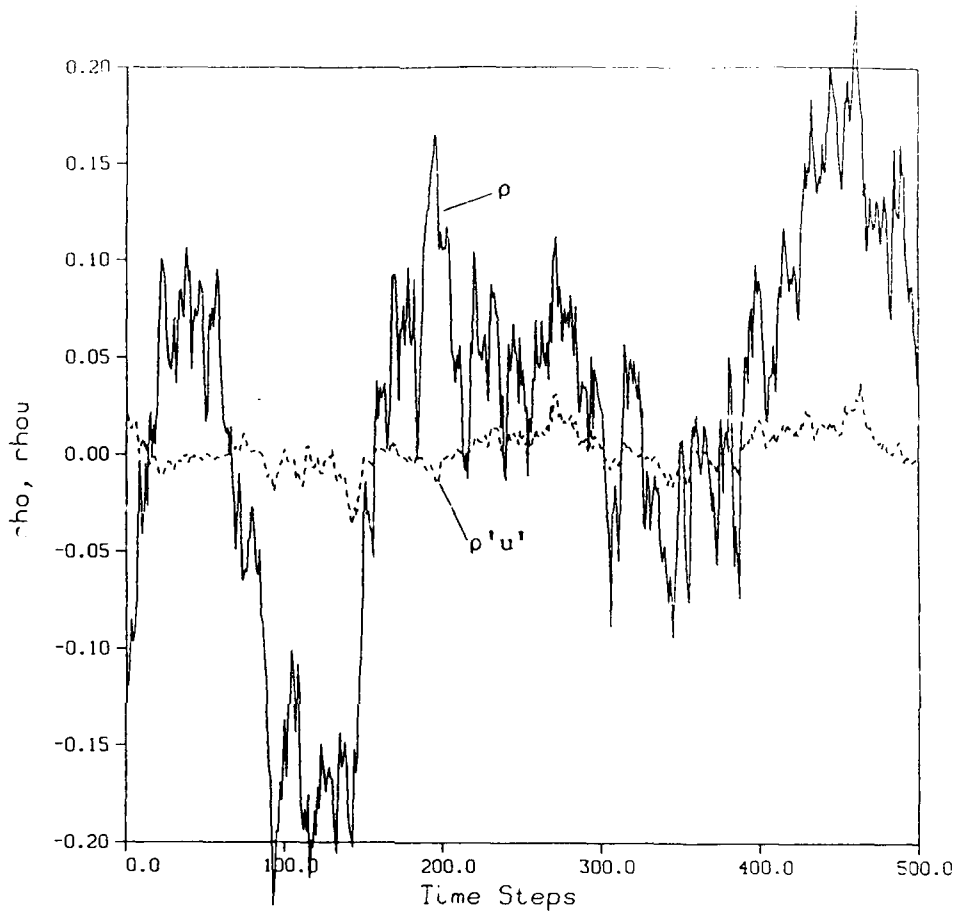

a. Time dependence of ρ and ρu.

Figure 6. Turbulence at the inflow boundary.

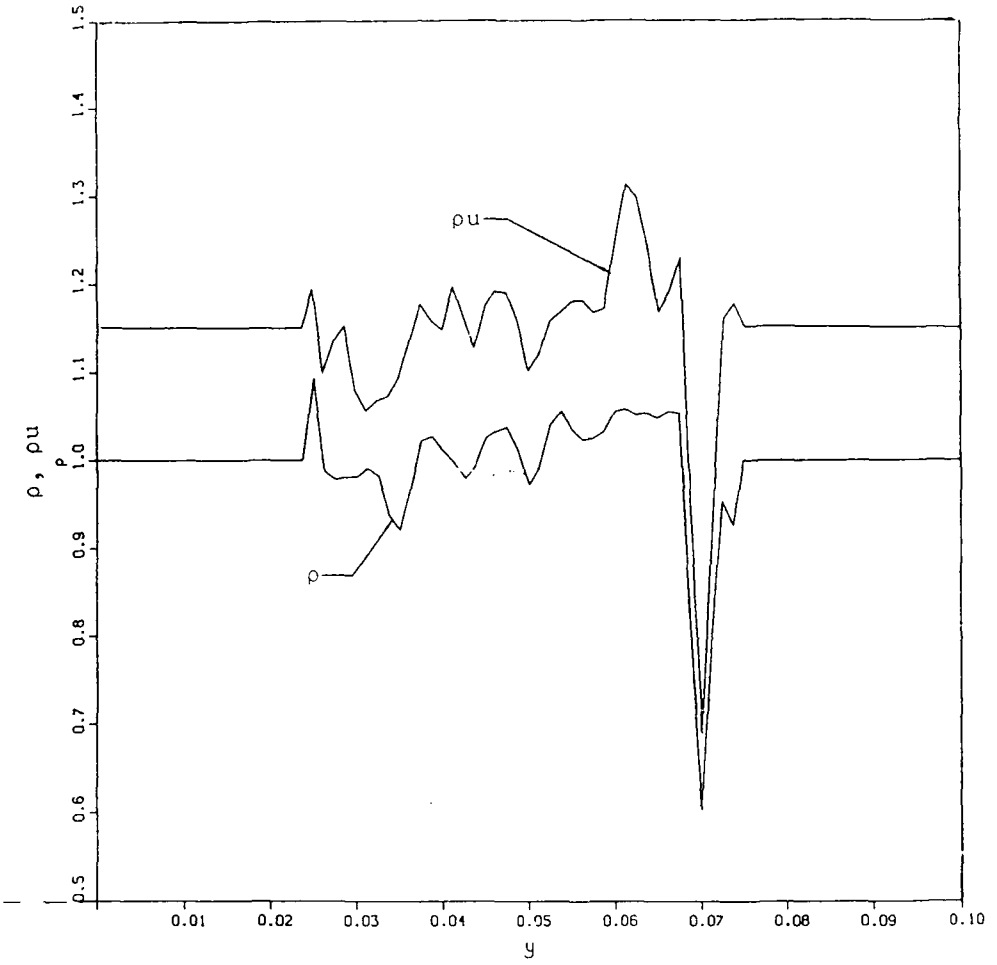

b. y- variation of ρ and ρu at t = 2000.

Figure 6. Concluded

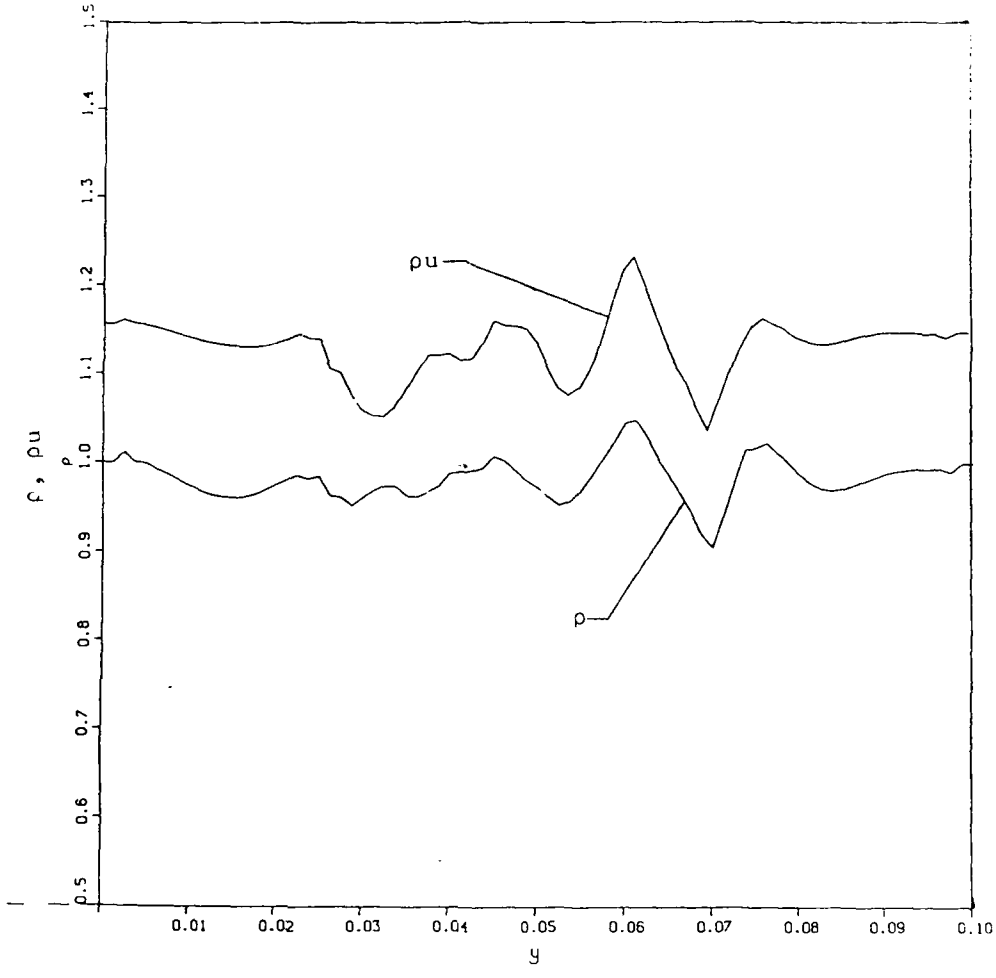

Figure 7. Turbulence in the flow field; y- variation of of ρ' and $\rho'u'$ at t=2000.

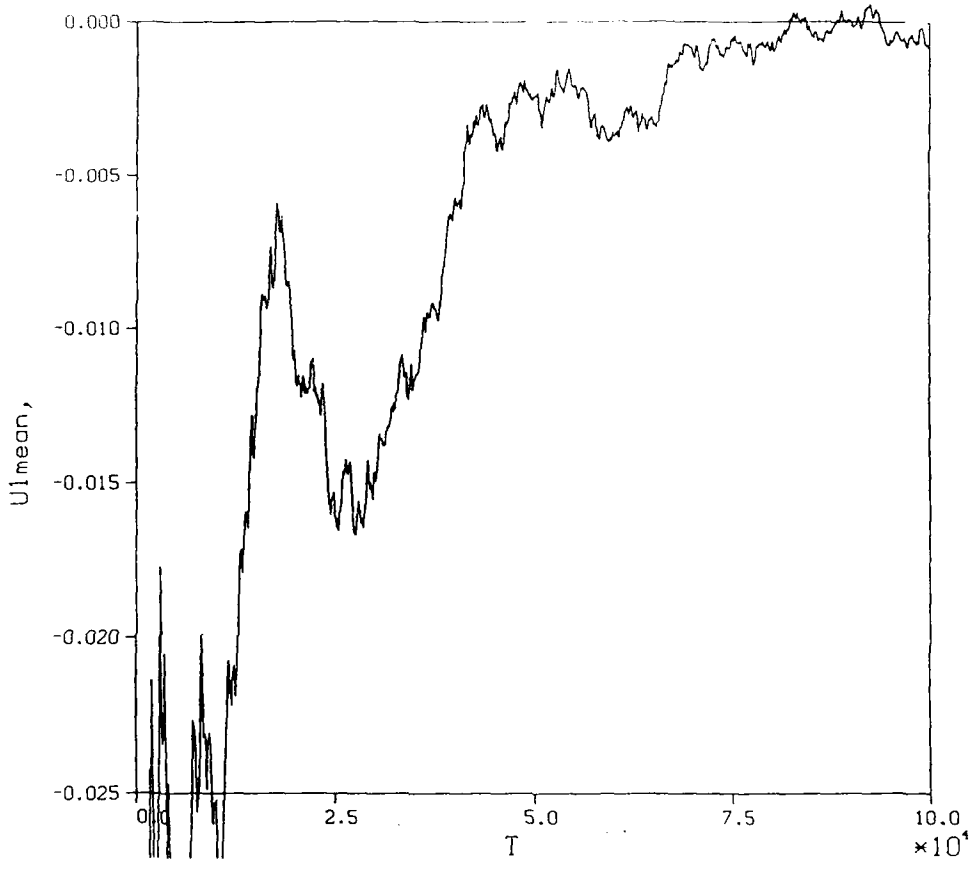

Figure 8. Plot of mean velocity fluctuation as a function of statistical ensemble size.

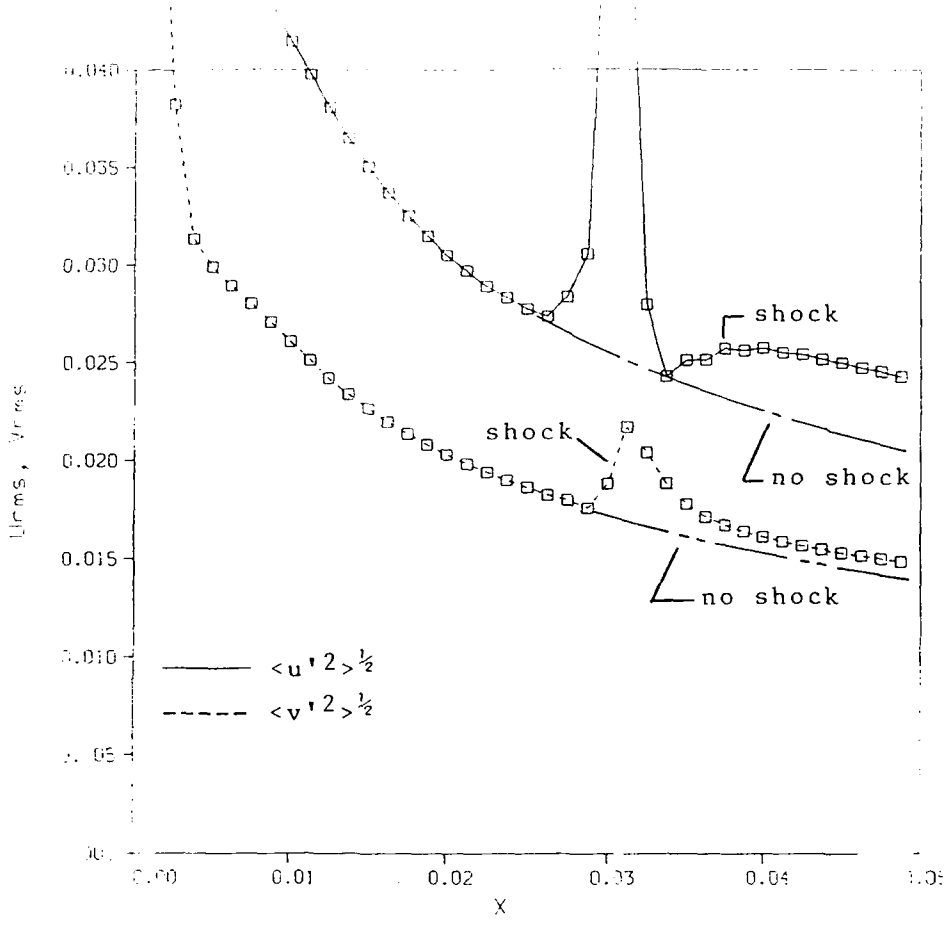

Figure 9. Statistics of turbulent velocity field through a shock.

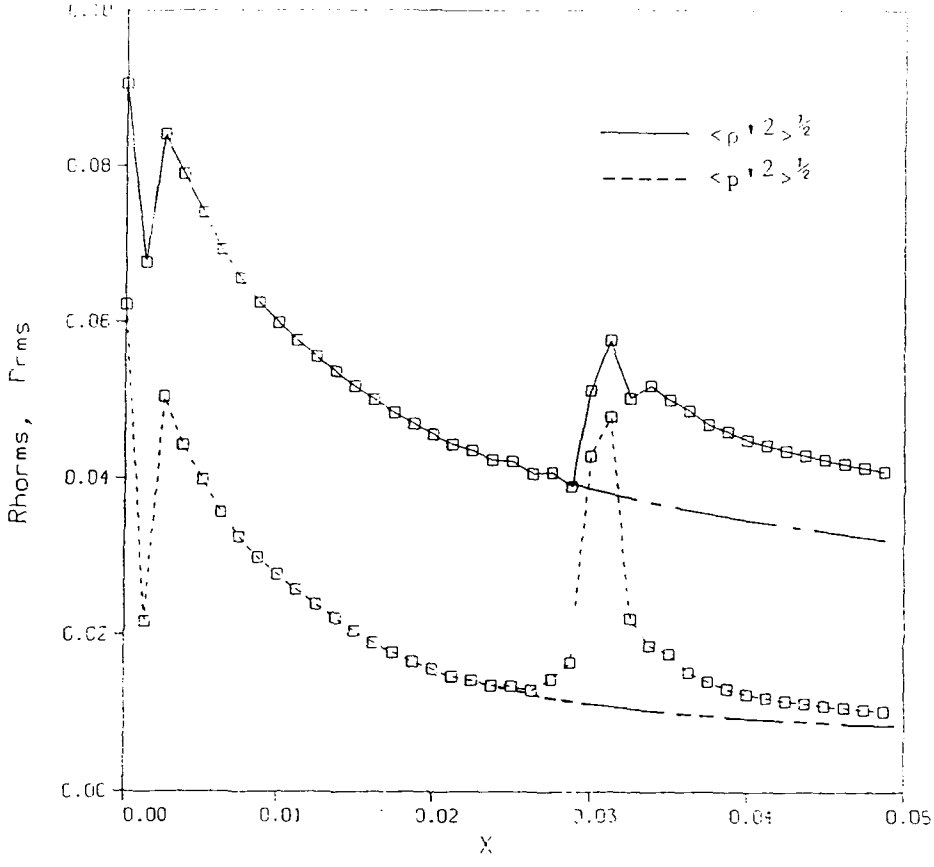

Figure 10. Statistics of pressure and density.

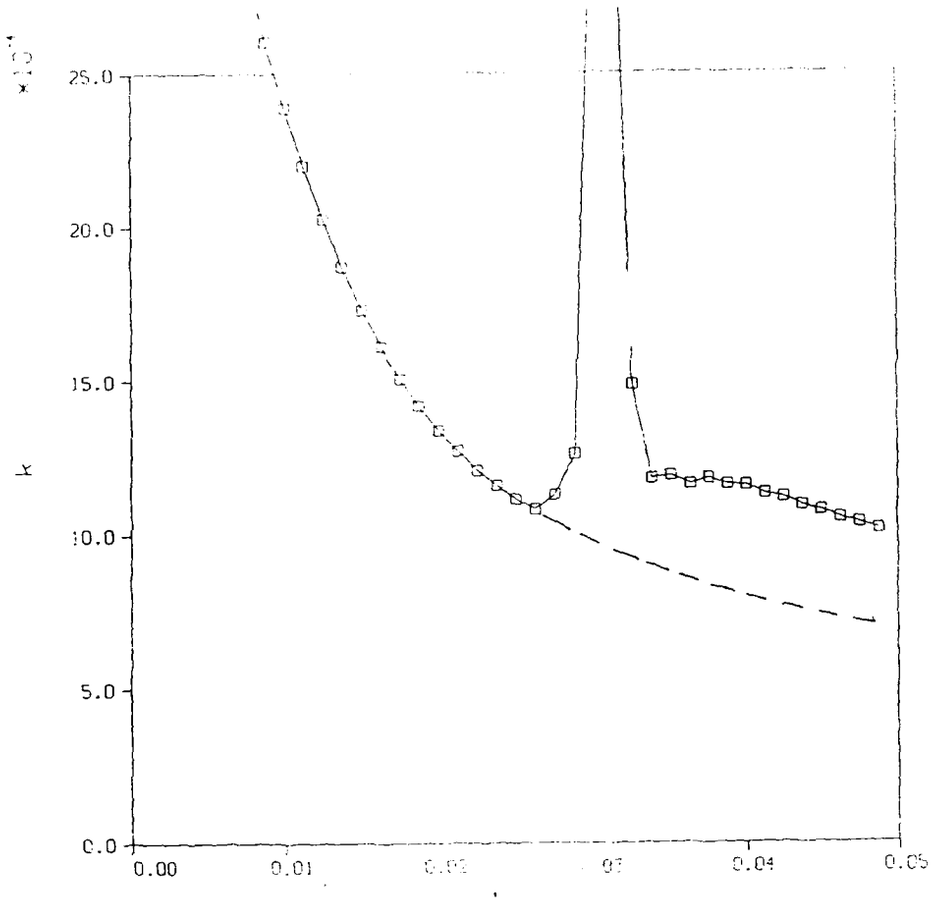

Figure 11. Statistics of turbulence kinetic energy.

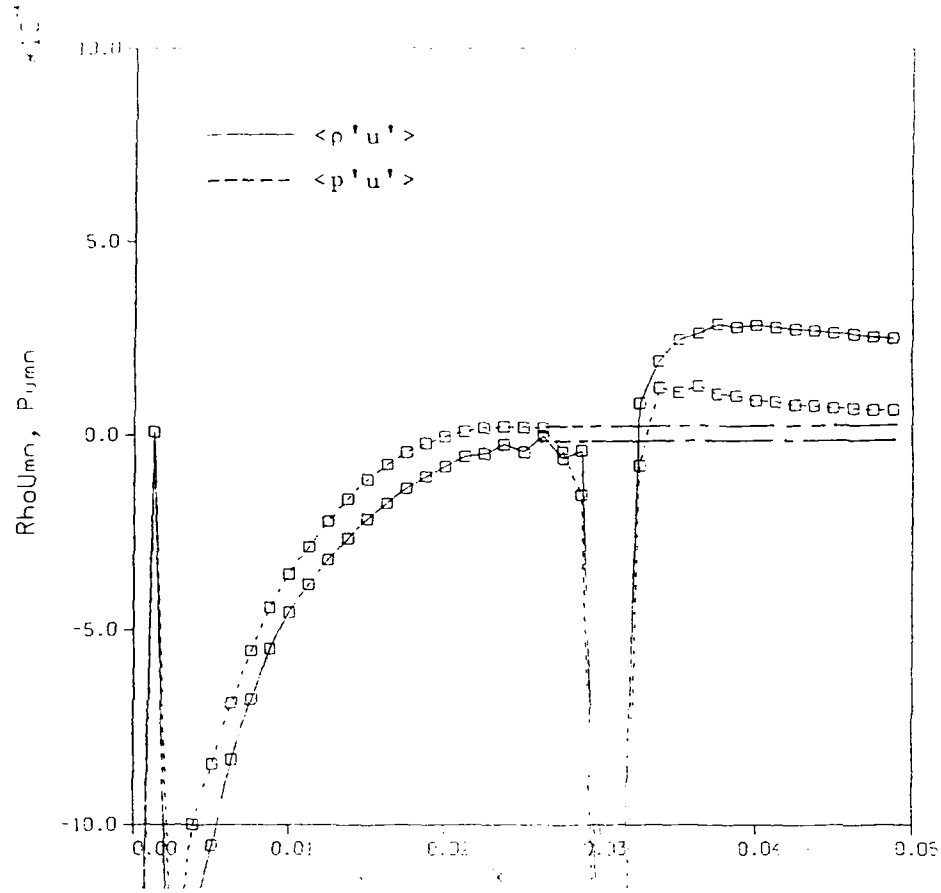

Figure 12. Statistics of ρ'u' and p'u'.

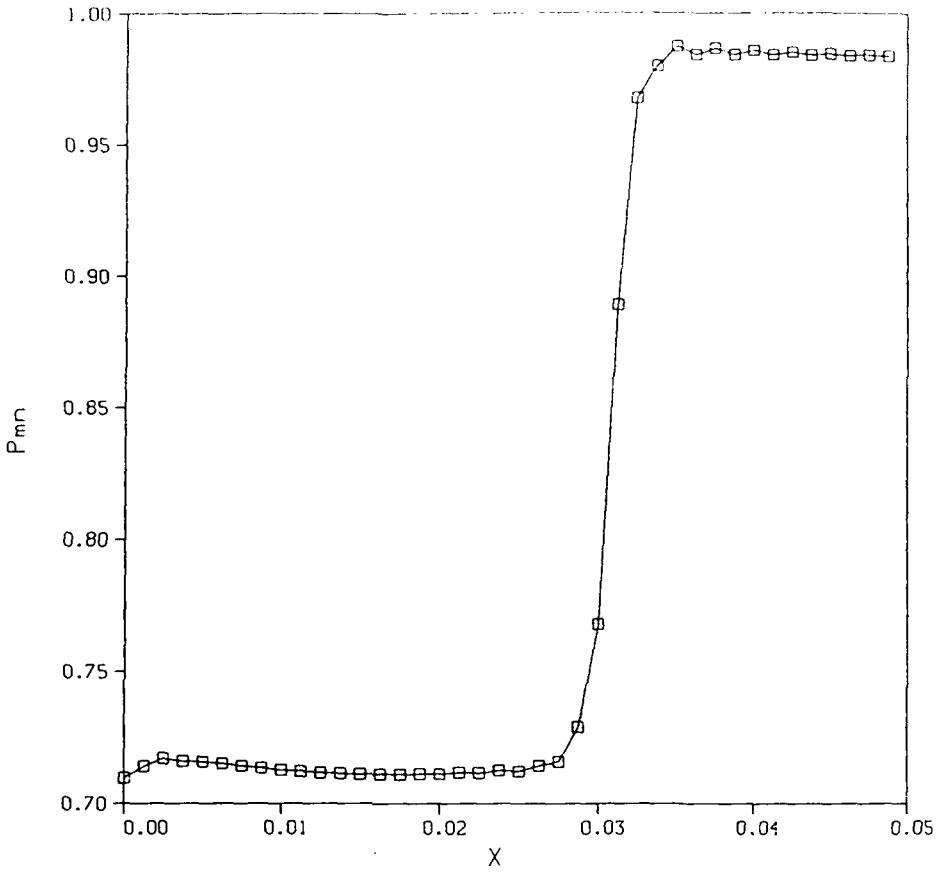

Figure 13. Distribution of mean pressure on 80x80 grid.

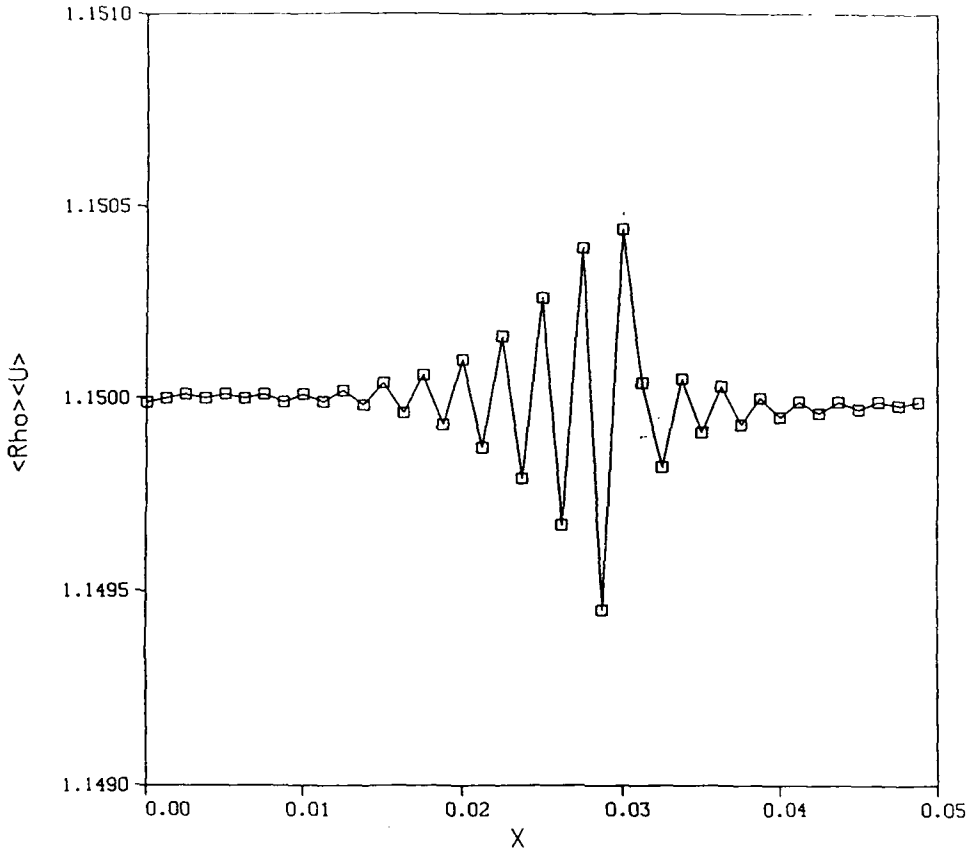

Figure 14. Plot of $<\rho><u>$ for steady flow with a shock wave.

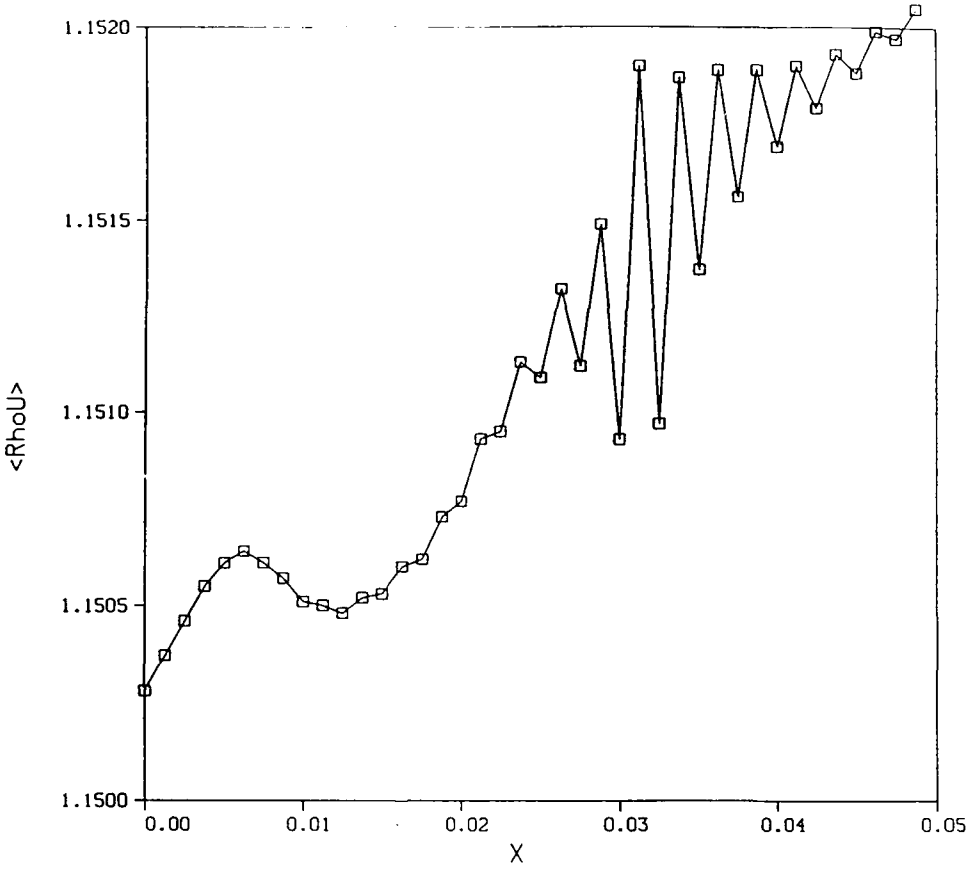

Figure 15. Plot of $<\rho u>$ for turbulent flow with a shock wave.

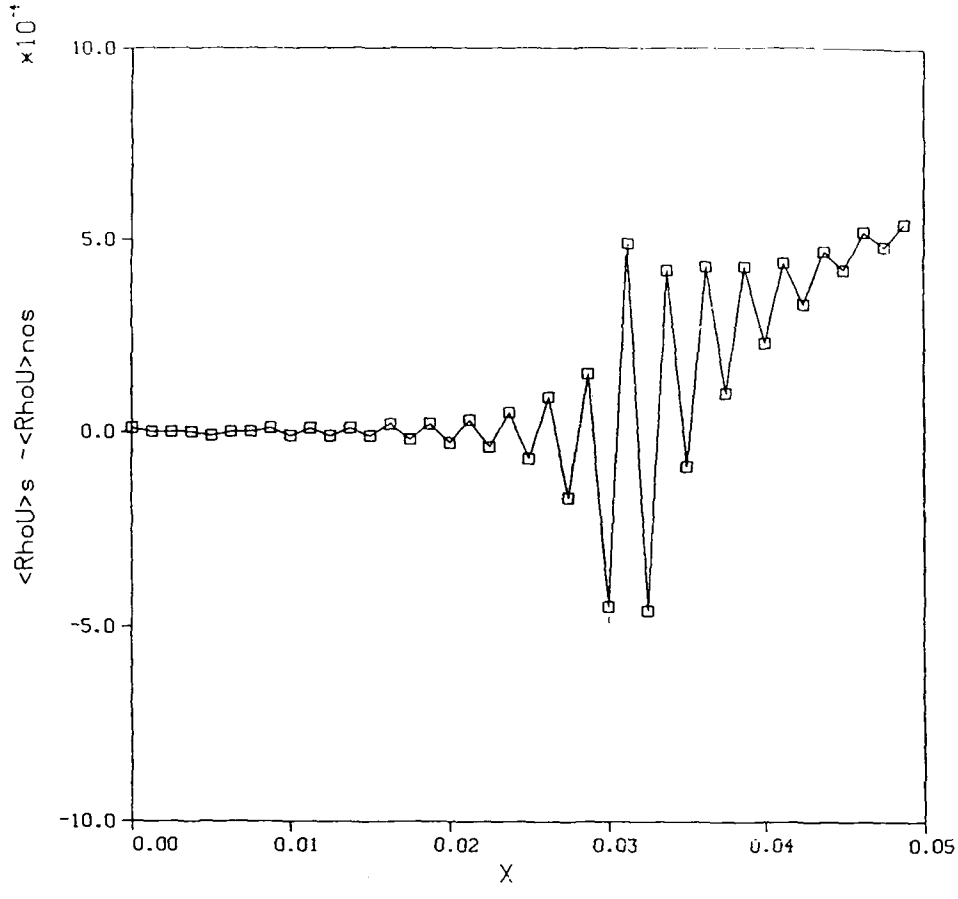

Figure 16. Plot of difference between mass flux for shock and no-shock.

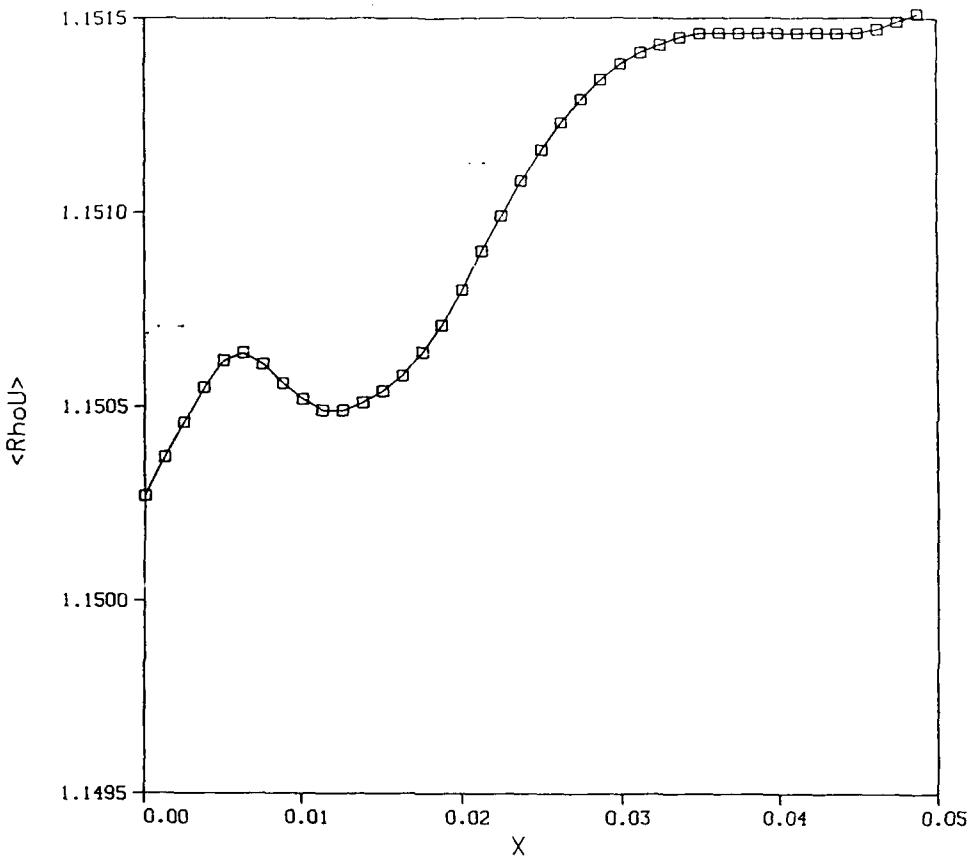

Figure 17. Plot of $<\rho u>$ for turbulent flow with no shock wave.

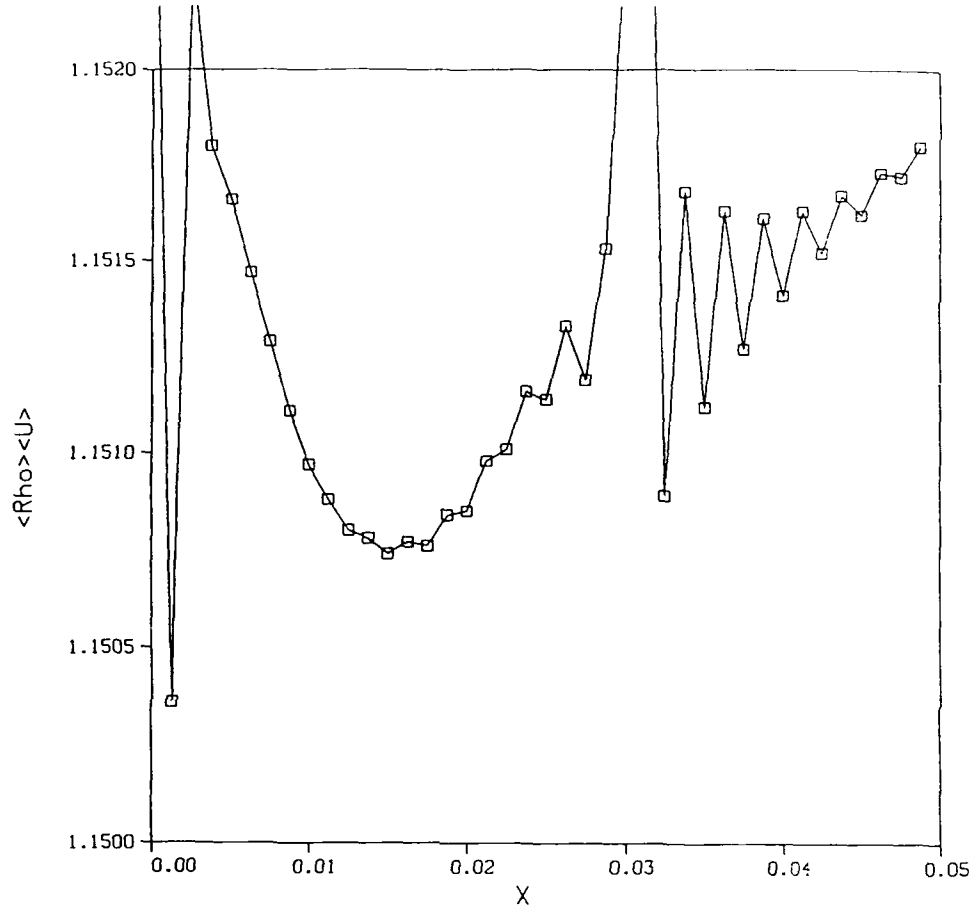

Figure 18. Plot of $<\rho><u>$ for turbulent flow with a shock wave.

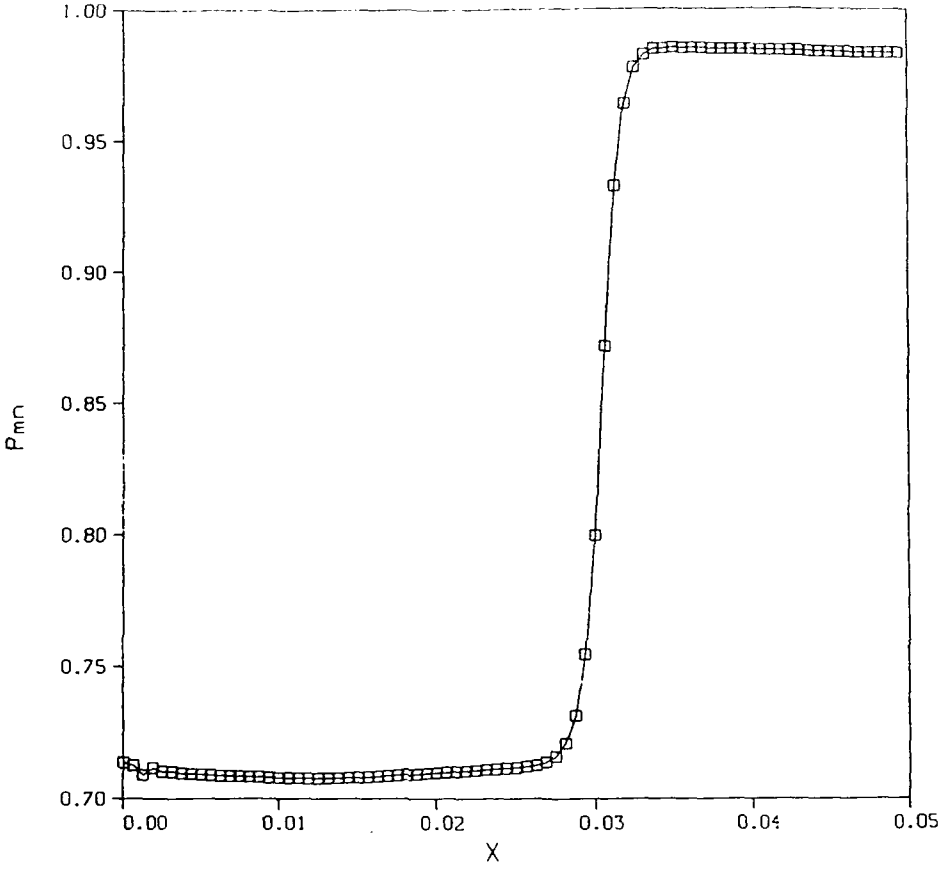

Figure 19. Distribution of mean pressure on 160x160 grid.

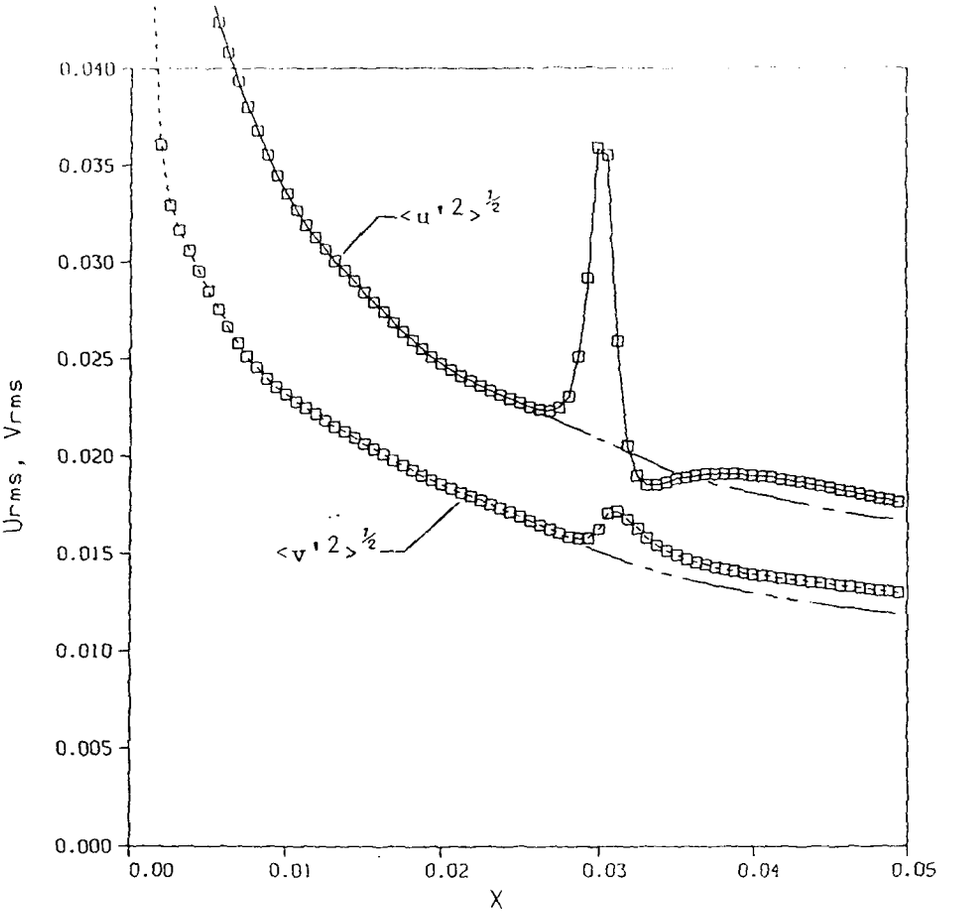

Figure 20. Statistics of turbulent velocity intensities on 160x160 grid.

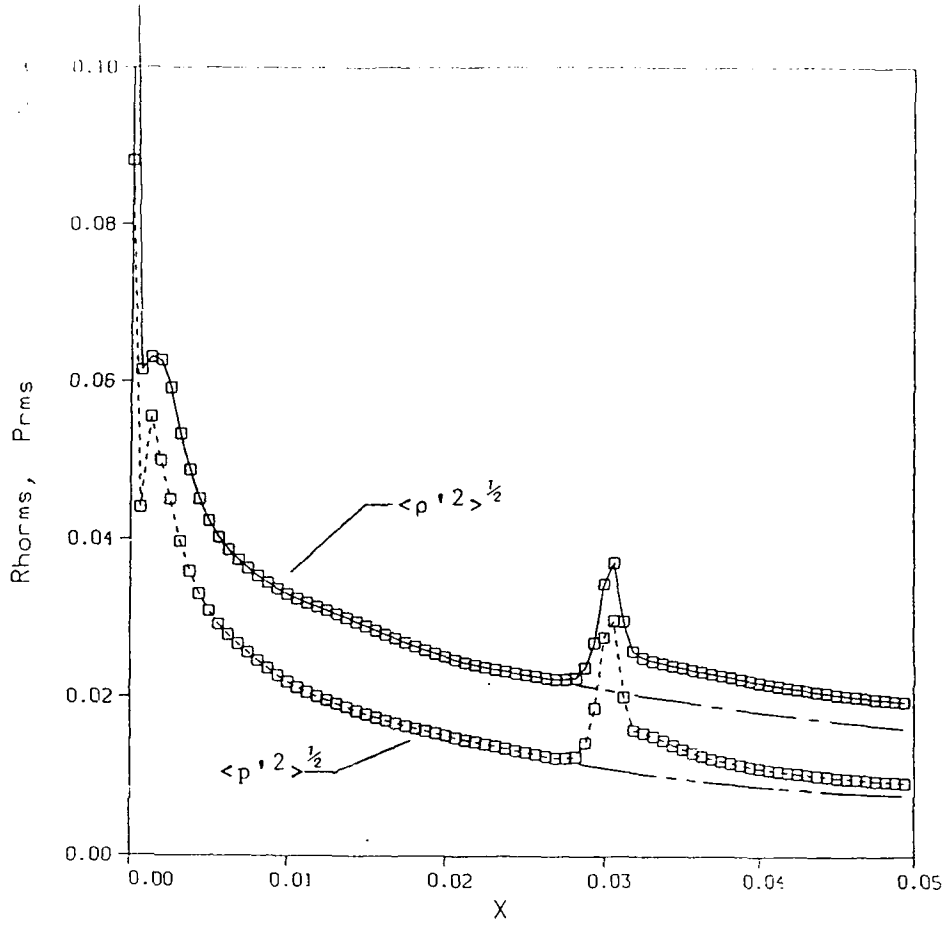

Figure 21. Statistics of pressure and density on 160x160 grid.

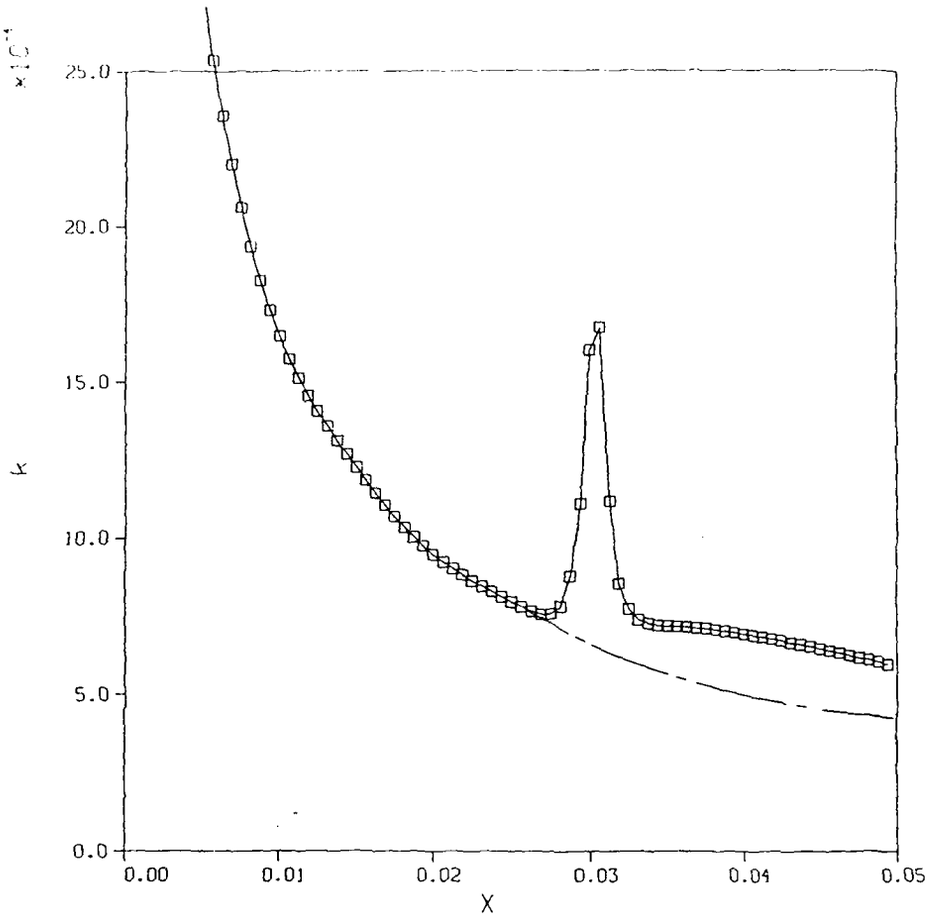

Figure 22. **Statistics of turbulent kinetic energy on 160x160 grid.**

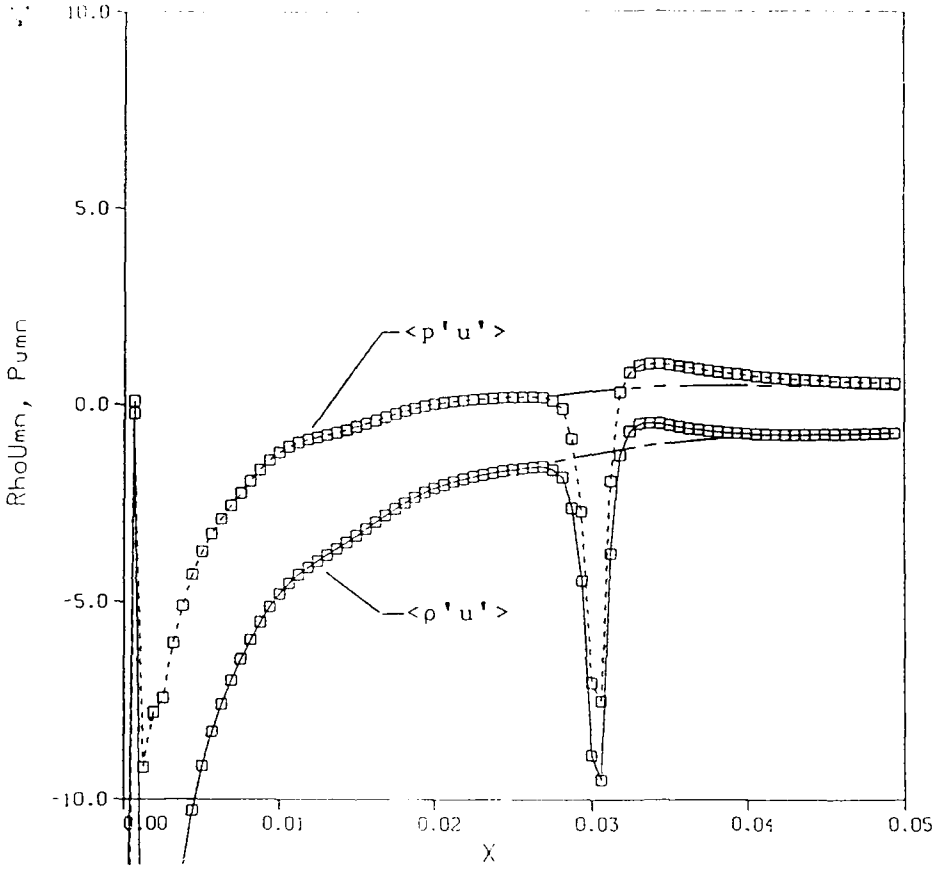

Figure 23. Statistics of ρ'u' and p'u' on 160x160 grid.

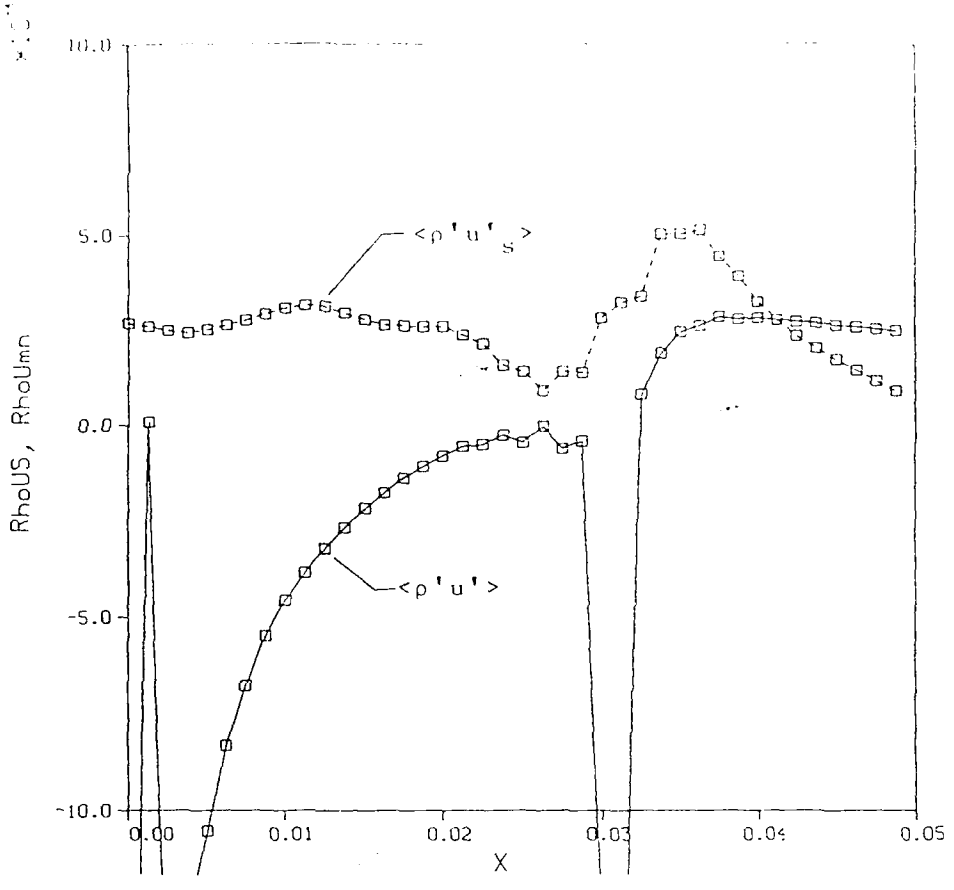

Figure 24. Comparison of $<\rho' u'>$ and $<\rho' u'_s>$

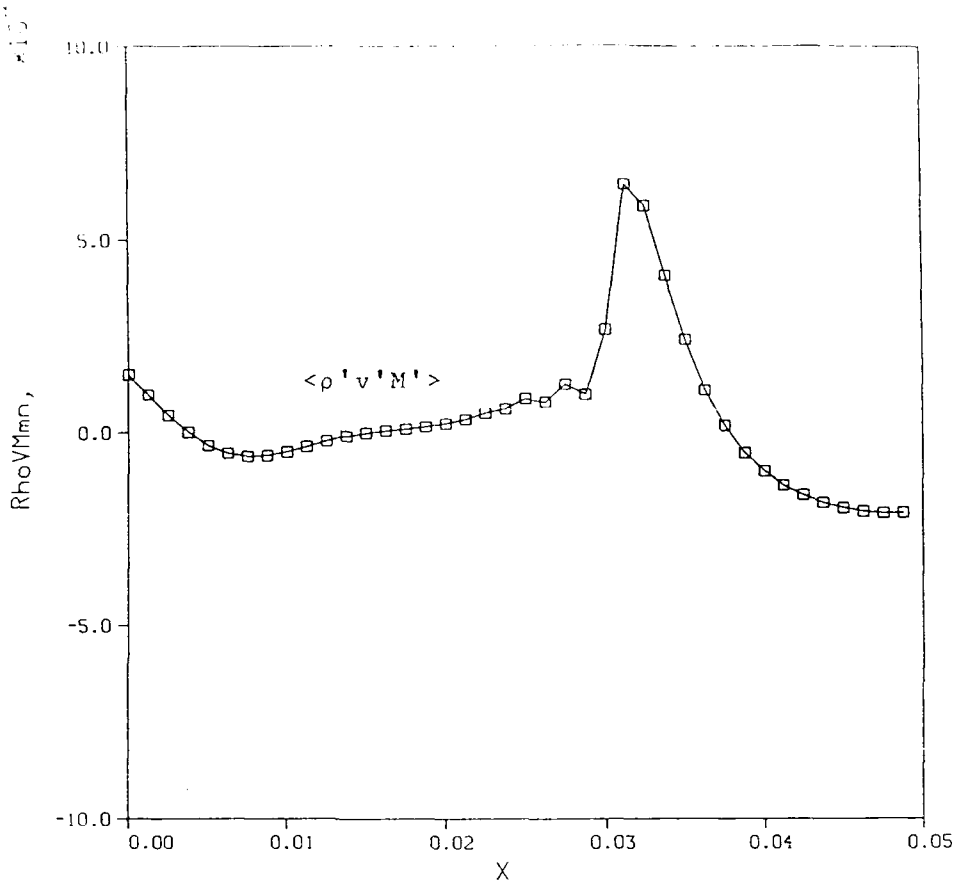

Figure 25. Shock ripple, ρv interaction distribution.

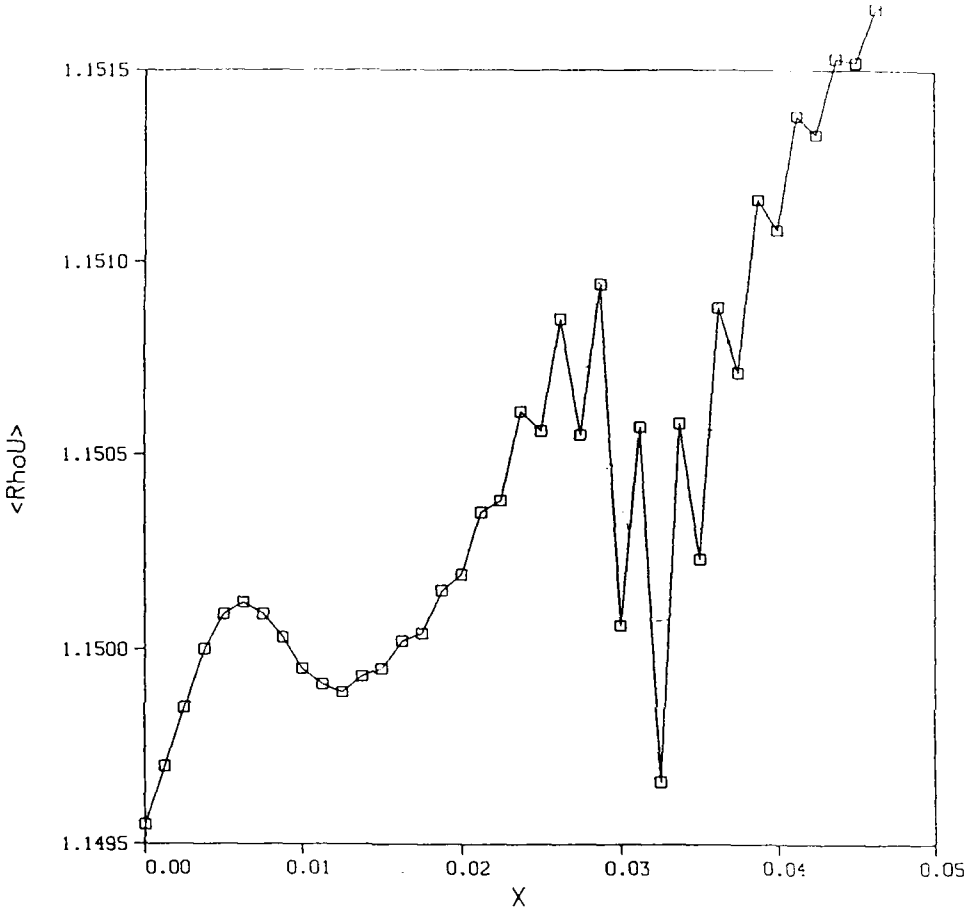

Figure 26. Plot of mass balance for turbulent flow with a shock wave.

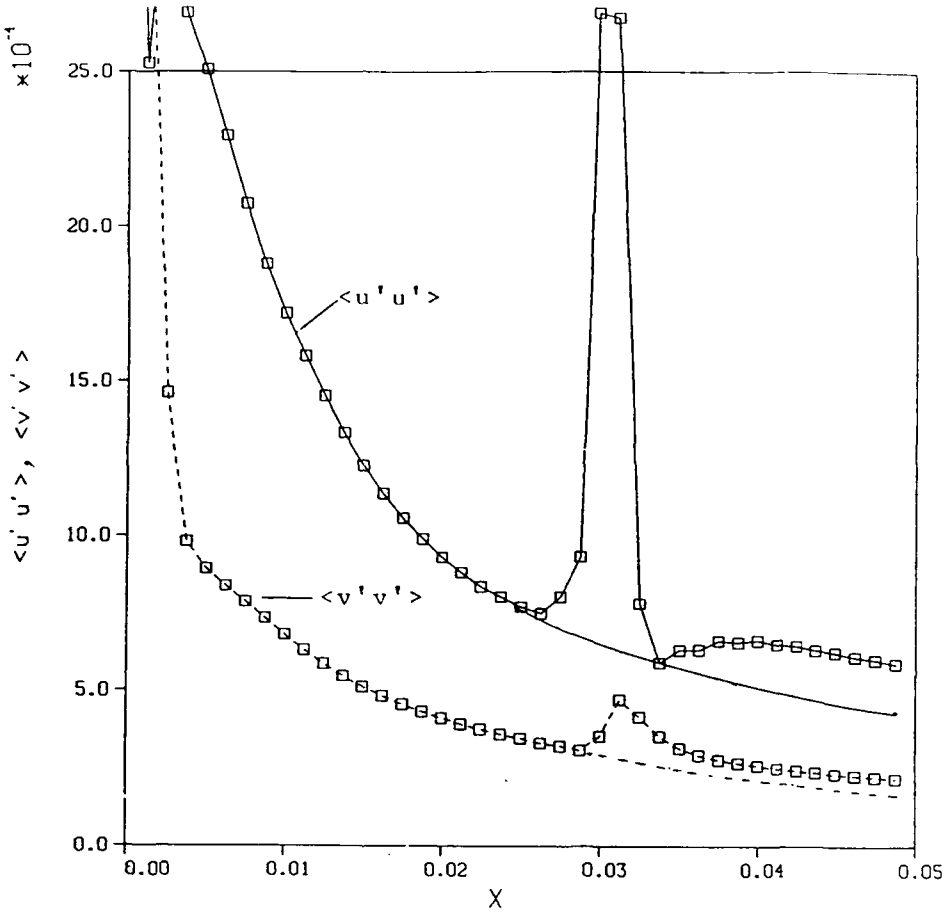

Figure 27. Plot of <u'u'> and <v'v'>.

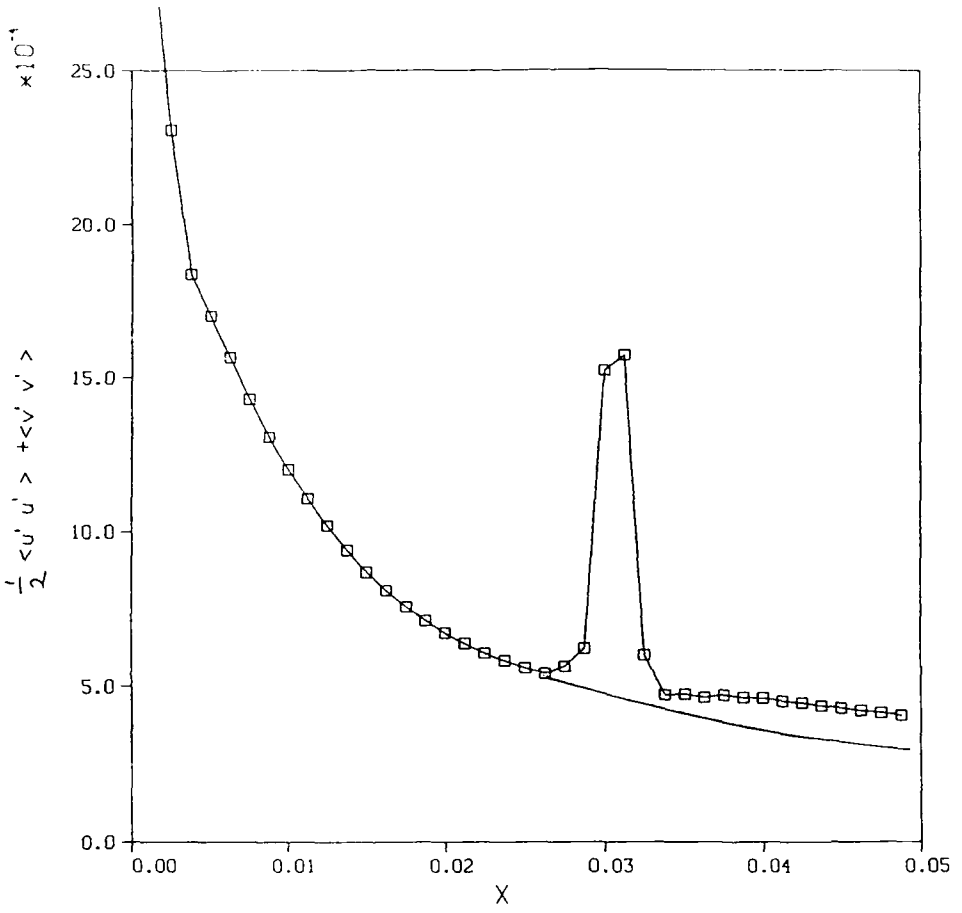

Figure 28. Plot of (<u'u'>+<v'v'>)/2.

APPENDIX A

ANALYSIS OF TURBULENT KINETIC ENERGY

Consider the conservation of mass through a normal shock wave, that is

$$\rho_1 u_1 = \rho_2 u_2 \tag{A1}$$

where ρ is the density and u is the velocity normal to the shock; the subscripts 1 and 2 denote values ahead of and behind the shock respectively.

The density can be written in the form

$$\rho = \rho_\infty \{1 + \frac{(\gamma-1)M_\infty^2}{2} (1 - \hat{u}^2)\}^{\frac{1}{\gamma-1}} \exp(-s/R) \tag{A2}$$

where $\hat{u}$ is the velocity normalized with respect to a reference velocity, u_∞, with an associated Mach number, M_∞; S is the entropy and R is the gas constant.

If the shock wave is weak, the entropy jump, ΔS, across the shock is given by

$$\Delta S/R = \frac{2\gamma}{3(\gamma+1)^2} (M_1^2 - 1)^3 = A(M_1^2 - 1)^3 \tag{A3}$$

where M_1 is the Mach number ahead of the shock wave.

Now let $\hat{u}$ be represented by

$$\hat{u} = 1 + u \tag{A4}$$

Using Equations (A2), (A3), and (A4), Equation (1) can be expanded to second order in u as

$$1 + \beta^2 u_1 - \frac{\kappa}{2} u_1^2 = (1 + \beta^2 u_2 - \frac{\kappa}{2} u_2^2) [1 - A(M_1^2 - 1)^3] \tag{A5}$$

where

$$\beta^2 = 1 - M_\infty{}^2$$

$$\kappa = M_\infty{}^2[3 + (\gamma-2)M_\infty{}^2] \tag{A6}$$

In this formulation M_1 is given by

$$M_1{}^2 = M_\infty{}^2 + \kappa u_1 \tag{A7}$$

The perturbation velocity can now be represented by

$$u = \bar{u} + u' \tag{A8}$$

where $\bar{u}$ is a stationary value and u' is a fluctuating value.

Now let

$$\bar{u}_1 = 0 \tag{A9}$$

and a zeroth order perturbation analysis gives

$$\beta^2\bar{u}_2 - \frac{\kappa}{2}\bar{u}_2{}^2 + A\beta^6 = 0 \tag{A10}$$

while a first order analysis gives

$$\beta^2 u_1' - \kappa u_1' u_1' = (\beta^2 u_2' - \kappa u_2' u_2')\{1 + [-\beta^6 - 3\beta^2(\kappa u_1')^2 + 3\beta^4 \kappa u_1' + (\kappa u_1')^3]\} \tag{A11}$$

If the shock is weak such that

$$\beta^2 << 1 \tag{A12}$$

then a first approximation to Equation (A11) is

$$\beta^2 u_1' - \kappa u_1' u_1' = \beta^2 u_2' - \kappa u_2' u_2' \tag{A13}$$

Now the above analysis assumes that the velocities are relative to the shock wave. If the shock wave is moving at speed u'_s and is at an inclination m, where

$$m = \frac{dx_s}{dy} \tag{A14}$$

then, in a fixed frame of reference

$$u' = (\hat{u}' - u_s' - m\bar{v} - mv')/(1 + m^2)^{1/2} \tag{A15}$$

where $\hat{u}$ is the fluctuating velocity in the fixed frame of reference, $\bar{v}$ is the mean value of v and v' is the fluctuating value of v. Using Equation (A15) in Equation (A13) and taking averages

$$\kappa[\langle\hat{u}_1'\hat{u}_1'\rangle - \langle u_s'\hat{u}_1'\rangle] + \beta^2\langle mv_1'\rangle = \kappa[\langle\hat{u}_2'\hat{u}_2'\rangle - u_s'\hat{u}_2'\rangle] + \beta^2\langle mv_2'\rangle \tag{A16}$$

where terms of order higher than the second have been neglected. Equation (A16) can be rearranged to give

$$\langle\hat{u}_1'\hat{u}_1'\rangle = \langle\hat{u}_2'\hat{u}_2'\rangle + [\langle u_s'\hat{u}_1'\rangle - \langle u_s'\hat{u}_2'\rangle] - \beta^2/\kappa\ [\langle m\hat{v}_1'\rangle - \langle m\hat{v}_2'\rangle] \tag{A17}$$

If the shock is stationary, then Equation (A17) reduces to

$$\langle\hat{u}_1'\hat{u}_1'\rangle = \langle\hat{u}_2'\hat{u}_2'\rangle \tag{A18}$$

For the tangential component of velocity the jump in $\hat{v}$ in shock fixed coordinates, gives

$$\hat{v}_1 = \hat{v}_2 \tag{A19}$$

and in space fixed coordinates

$$\hat{v}_1 + (\hat{u}_1 - u_s)m = \hat{v}_2 + (\hat{u}_2 - u_s)m \tag{A20}$$

Again splitting v into a stationary and non-stationary component gives

$$\hat{v}_1' + (\hat{u}_1' - u_s')m = \hat{v}_2' + (\hat{u}_2' - u_s)m \tag{A21}$$

squaring both sides, neglecting terms of order higher than the second and averaging gives

$$\langle \hat{v}_1' \hat{v}_1' \rangle = \langle \hat{v}_2' \hat{v}_2' \rangle \tag{A22}$$

Using Equation (A17) and (A22) it may be seen that the jump in turbulent kinetic energy, defined by

$$k = \frac{1}{2} \{\langle u'u' \rangle + \langle v'v' \rangle\} \tag{A23}$$

is given by

$$k_1 - k_2 = \frac{1}{2} \{[\langle u_s' u_1' \rangle - \langle \hat{u}_s' \hat{u}_s' \rangle] - \beta^2/\pi[\langle m\hat{v}_1 \rangle - \langle m\hat{v}_2' \rangle]\} \tag{A24}$$

and it may be noted that if the shock speed and ripple terms are neglected, then k is continuous through a shock wave.

If the data from the simulations are used to evaluate the right hand side of Equation (A24) then

$$k_1 - k_2 = -2.31 \times 10^{-4} \tag{A25}$$

which is an increase of turbulent kinetic energy through the shock. In the simulation, k, as defined in Equation (23), is 5.56×10^{-4} and, hence, the shock increases k by 41%.

APPENDIX B

INDICIAL ANALYSIS

Since the flow conditions being used in these investigations are in the transonic range, it was suggested that some insight for assessing the magnitude of the effect of perturbations on the shock speed and the influence of the shock speed on the turbulence might be possible from a linear theory such as the transonic indicial theory developed by Nixon (Refs. B1 and B2).

The indicial method uses the principle of superposition to relate complex motions to an indicial response by means of Duhamel's integral. The indicial response is the time history of the motion in question in response to a step change in some flow parameter.

The basic equation for shock movement is, from Reference B1

$$\delta X_s(t) = \delta X_{s_\epsilon}(t)\epsilon(0) + \int_0^t \delta X_{s_\epsilon}(\tau)\,\frac{d\epsilon(t-\tau)}{dt}\,d\tau \qquad \text{(B1)}$$

where δX_s is the shock movement, and $\epsilon(t)$ is a time-dependent parameter typifying the unsteady motion. $\delta X_{s\epsilon}(t)$ is the indicial response, defined as the response of the shock location due to the instantaneous unit change in the parameter $\epsilon(t)$. In Reference B2, Nixon shows that for an input representing simple harmonic motion, the shock motion is also harmonic, with a phase lag varying with the frequency of the driving function. In particular, for very high frequencies, the shock motion goes to zero as 1/k where k is the reduced frequency, $\omega c/u_\infty$, where c is a reference length and u_∞ is the freestream velocity. However, while the magnitude of the shock movement vanishes as frequency increases, the theory indicates that the velocity of the motion remains oscillatory with a finite amplitude while the amplitude of the acceleration of the shock motion approaches ∞ as the reduced frequency.

The above discussion suggests that an important part of the turbulence in a shock/turbulence interaction may be the motion of the shock itself, which is not accounted for by the Reynolds averaging process which averages the fluctuating

quantities over a long time and considers only fluctuations of the flow velocities and other flow variables relative to a fixed coordinate system. In order to obtain an estimate of the magnitude of the shock motion corresponding to the numerical experiments discussed previously, a series of calculations were made for a case using the indicial theory.

In the indicial test cases, the same type of flow configuration was used as for the results shown in Figures 9-17. However, instead of imposing a random variation of the flow variables in the center portion of the inflow boundary, two cases were calculated. The first case was the indicial response case in which all flow variables were held constant at their initial values on the inflow boundary except for the streamwise velocity component, u, which was given a step perturbation at time zero in the center portion of the boundary (40 grid points) and held at the perturbed value for the entire calculation. In the second case, the u-velocity component was calculated from the random function in time, the same value being specified at all y locations on the inflow boundary for each time step. In other words, the inflow was a two-dimensional pulse with random fluctuations.

Typical results from the indicial response calculation are shown in Figures B1-B3. In Figure B1, contours of constant pressure are shown 1000 time steps after the initial step perturbation of the inflow velocity. In Figure B2, a composite plot is shown of the pressure distributions along constant x lines near the centerline of the flow. The initial pressure distribution of the unperturbed flow is shown for comparison. Finally, in Figure B3, the indicial shock displacement from the initial location is shown. There is a short delay from the start of the calculation, corresponding to the propagation of the step pulse through the upstream flow, then the shock begins to move in response to the new inflow. The waviness of the shock motion is a numerical phenomenon related to the size of the computational grid, the small number of grid points in the shock capture region, and the linear interpolation of pressure which was used to locate the shock. For the calculations shown here, the shock location was taken to be the point where the pressure was equal to 0.85 and was rising with increasing x.

The fluctuating inflow velocity is shown in Figure B4. This function was imposed at the same 40 points in the center portion of the inflow boundary as was the step pulse in the indicial calculation. Two typical pressure contour plots are shown in Figure B5 for this case. The first, Figure B5a, shows the situation after 200 time steps, the second shows the situation after 1000 steps. Finally, the distribution of pressure along x lines near the centerline for the perturbed flow is shown in Figure B6a and b for the same two time steps as the previous figure.

The motion of the shock at the centerline was determined for the perturbed flow in the same manner as for the indicial flow, and the location of the shock as a function of time is shown in Figure B7. It is noted that the shock motion does not oscillate about zero as a mean value. The reason for this is that the input velocity perturbation (Fig. B4) does not oscillate about zero as a mean. While the perturbation of the velocity should eventually have zero mean value, the nonzero value apparent in Figure B5 is believed to be due to the small sample size. If the calculation were to be extended to include 10000 time steps, the true statistical mean should be apparent. The present analysis makes use of the small sample size because the interest is in the transient phenomena, not in the asymptotic statistics.

The shock perturbation velocity calculated by differencing the X_s data is shown in Figure B8. It is noted that the magnitude of the shock velocity is of the same order as that of the inflow velocity fluctuations. The shock motion appears smoother than the inflow velocity, due to the damping effects of the viscosity, both real and artificial, which reduces the higher frequency fluctuations in the calculated flow field.

With the apparent conceptual agreement between the full Navier-Stokes solution and the analytical indicial theory regarding the magnitude of the shock velocity and its potential importance to the shock/turbulence interaction, an examination was made of the ability of the indicial theory to predict the shock motion. Recalling Equation (B1), an equation for the shock velocity can be obtained by differentiation. Thus,

$$u_s(t) = \delta X_{s_\epsilon}(t)\,\frac{d\epsilon(0)}{dt} + \delta u_{s_\epsilon}(t)\,\epsilon(0) + \int_0^t \delta X_{s_\epsilon}(\tau)\,\frac{d^2\epsilon(t-\tau)}{dt^2}\,d\tau \qquad \text{(B2)}$$

The indicial response was shown in Figure B3. The function $\epsilon(t)$ was taken to be the inflow perturbation velocity, u(t), shown in Figure B4. Calculation of the integral in Equation (B2) by a simple trapezoidal rule and the derivative of the indicial response by backward differences produced the distribution of the shock velocity shown in Figure B9. Comparison of Figures B9 and B8 reveals that the shock velocity predicted by the indicial formulation has generally the same frequency and phase as that given by the Navier-Stokes solution, with large errors in the amplitude of the velocity fluctuations; the reason for the errors is not clear at present. The shock location determined by integration of Figure B9 compares fairly well with the direct solution (Fig. B10).

From the surprisingly good agreement between the indicial theory and the Navier-Stokes solution for the shock location, it can be tentatively concluded that the assumption of a linear relationship between certain flow properties and small perturbations of velocity, pressure, or density can be a useful tool for providing some insight to even the complex interaction between a shock and a turbulent flow field. For the present, the primary conclusion that can be drawn is that the shock motion must be included in any analysis of turbulence models for flows with shocks.

REFERENCES

B1. Nixon, D.: Notes on the Indicial Method, AIAA Journal, Vol. 16, No. 6, June 1978, pp. 613-616.

B2. Nixon, D.: On Unsteady Transonic Shock Motions, AIAA Journal, Vol. 17, No. 10, June 1979, pp. 1143-1145.

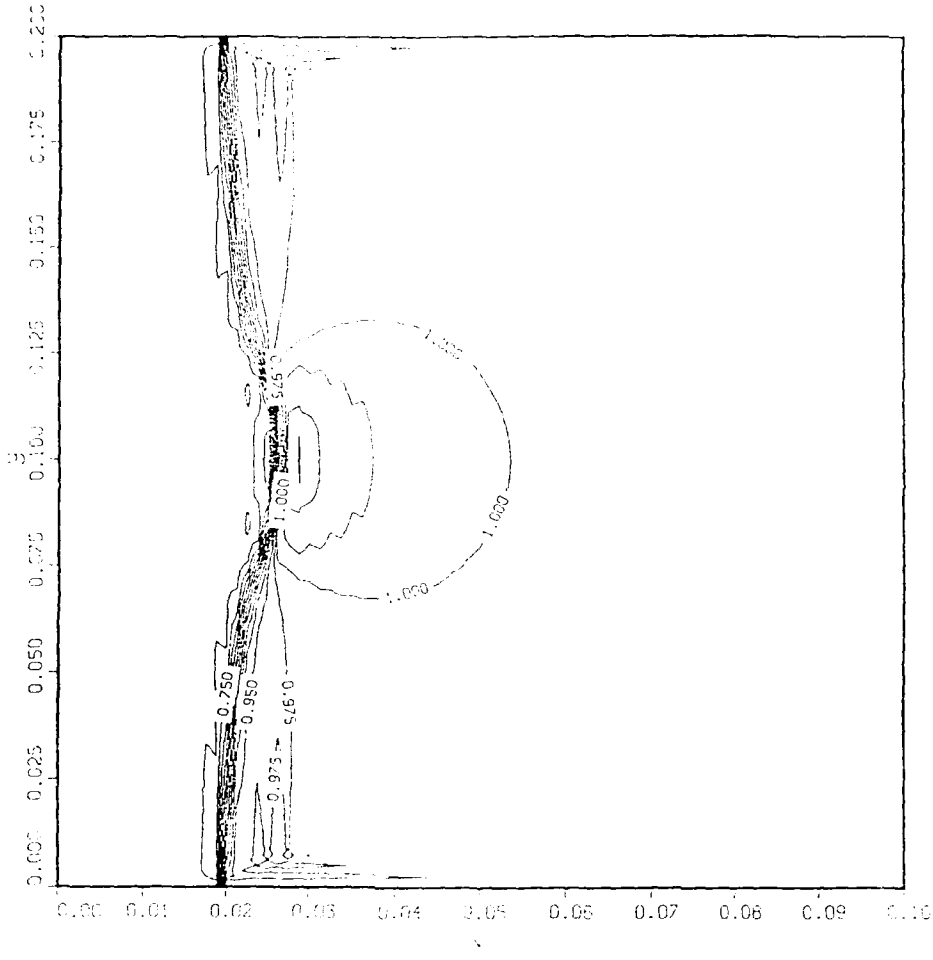

Figure B1. Contours of constant pressure for indicial solution.

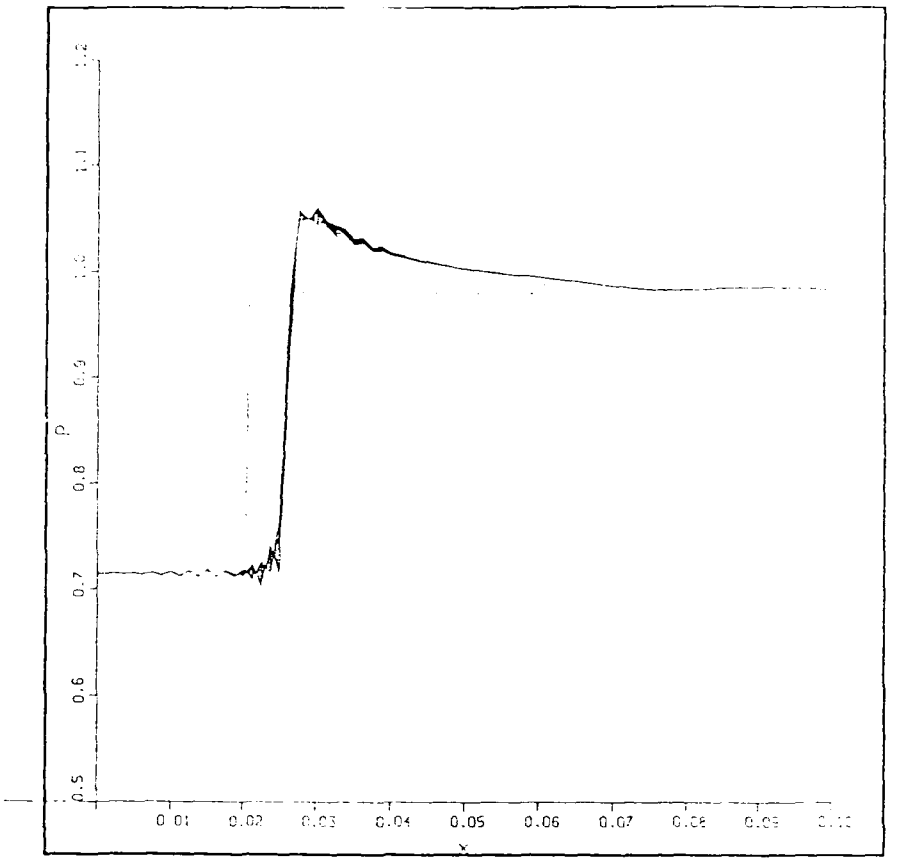

Figure B2. Pressure distribution near centerline for indicial solution.

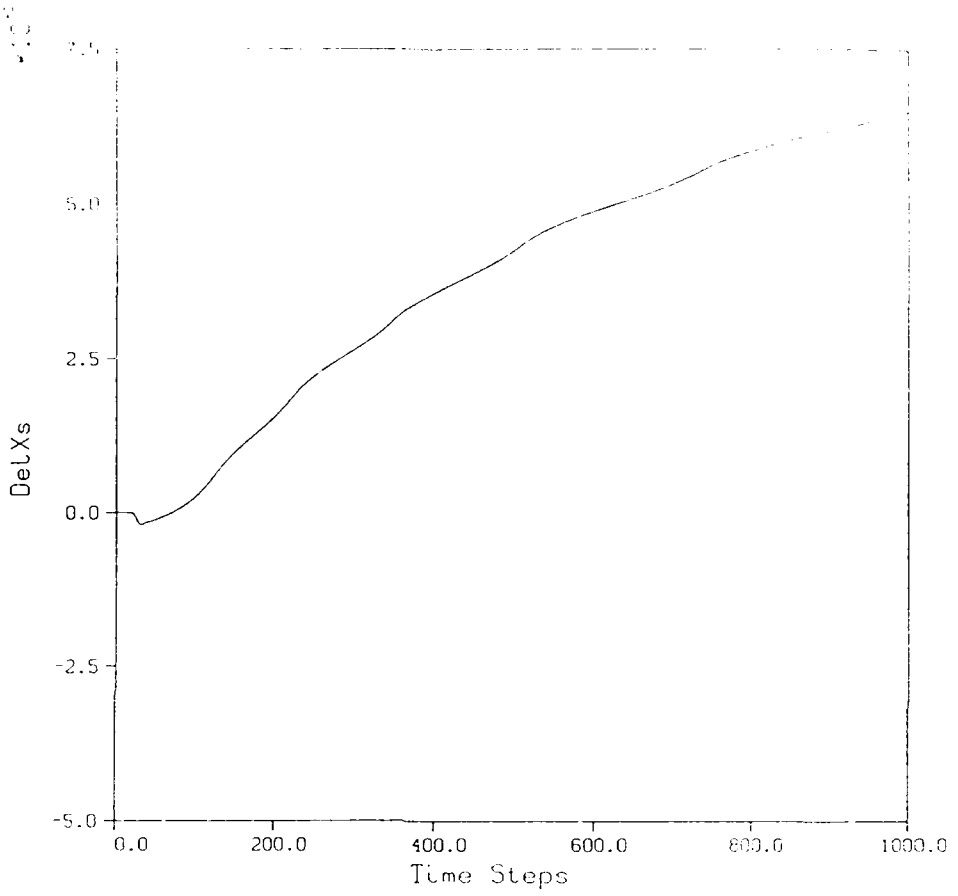

Figure B3. Plot of δX_s from indicial solution.

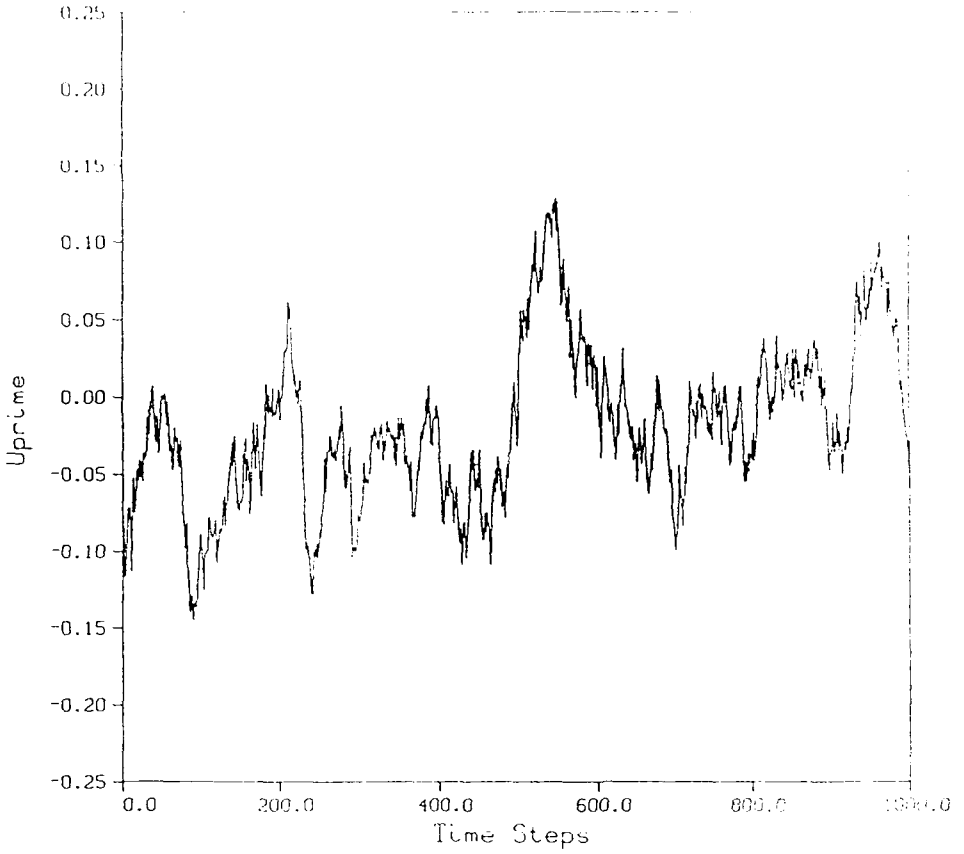

Figure B4. Plot of u from random function.

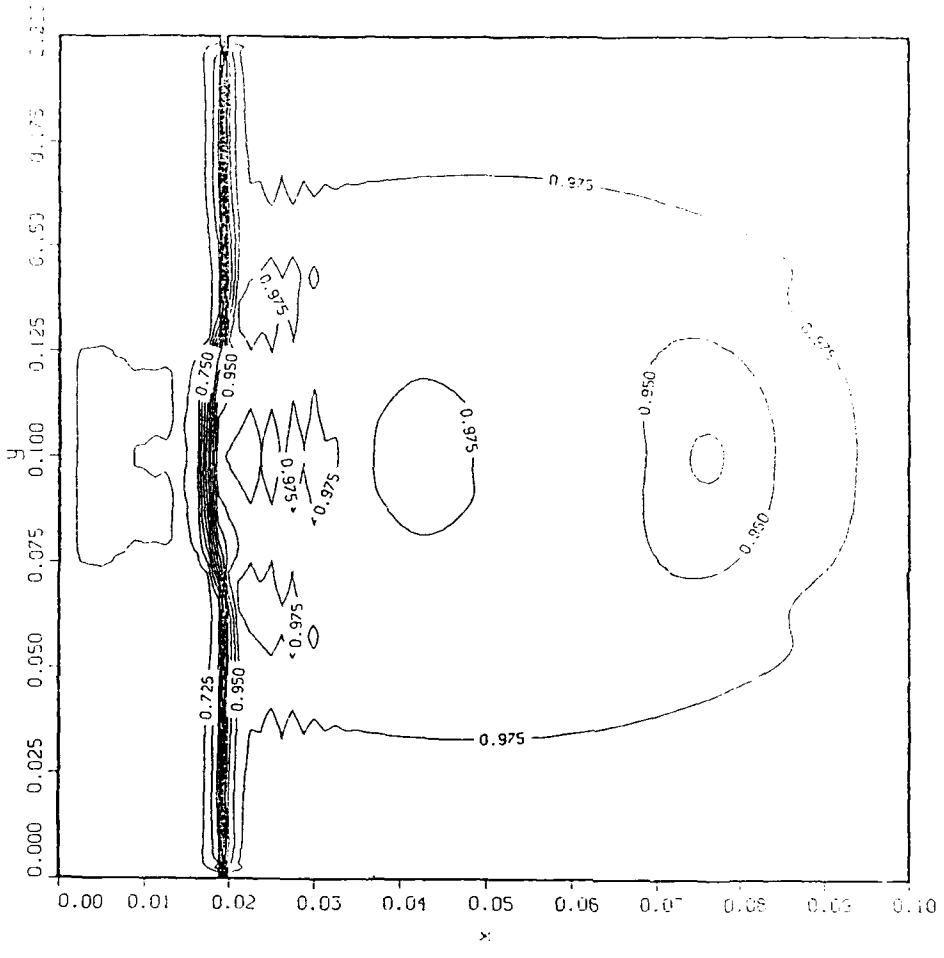

a. t = 200.

Figure B5. Contours of constant pressure for perturbed solution.

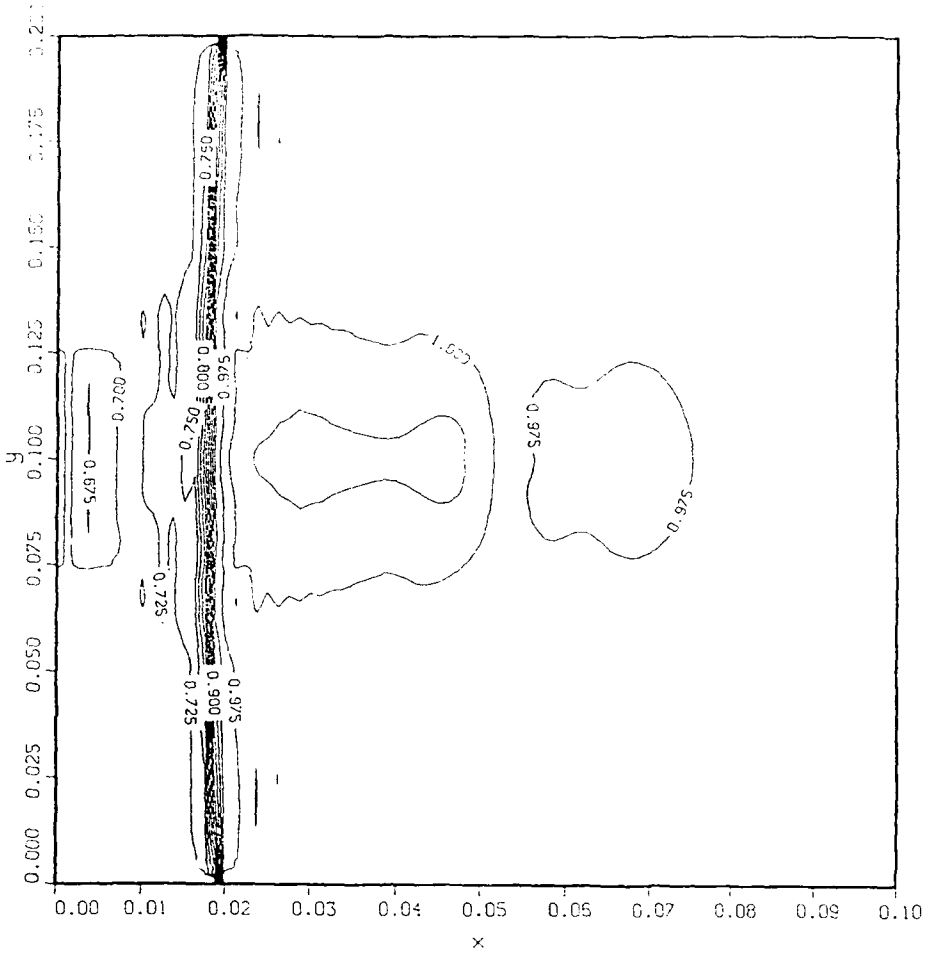

b. t = 1000.

Figure B5. Concluded

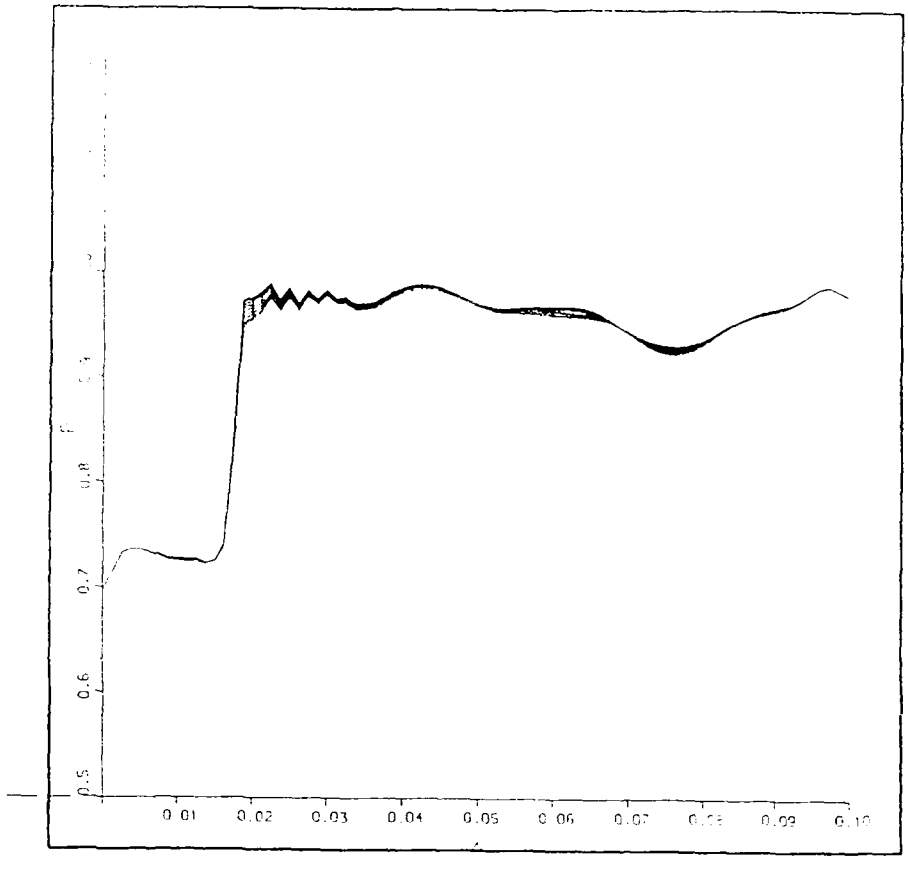

a. t = 200.

Figure B6. Pressure distribution near centerline for perturbed solution.

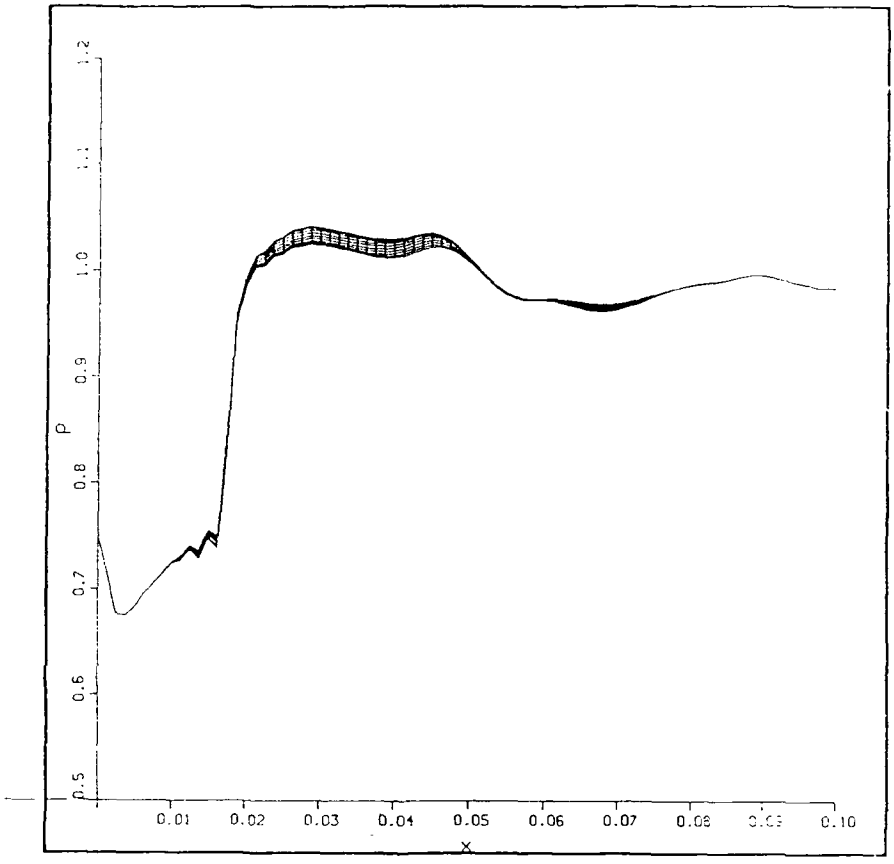

b. t = 1000.

Figure B6. Concluded

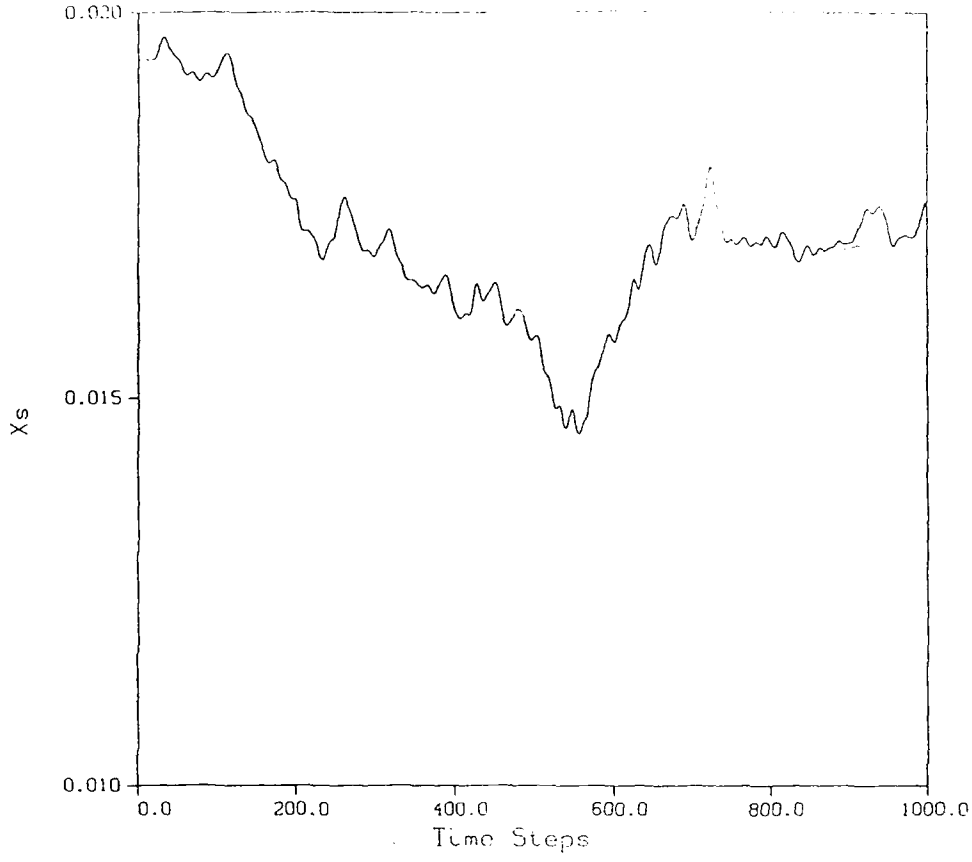

Figure B7. Plot of X_s from Navier-Stokes solution for perturbed case.

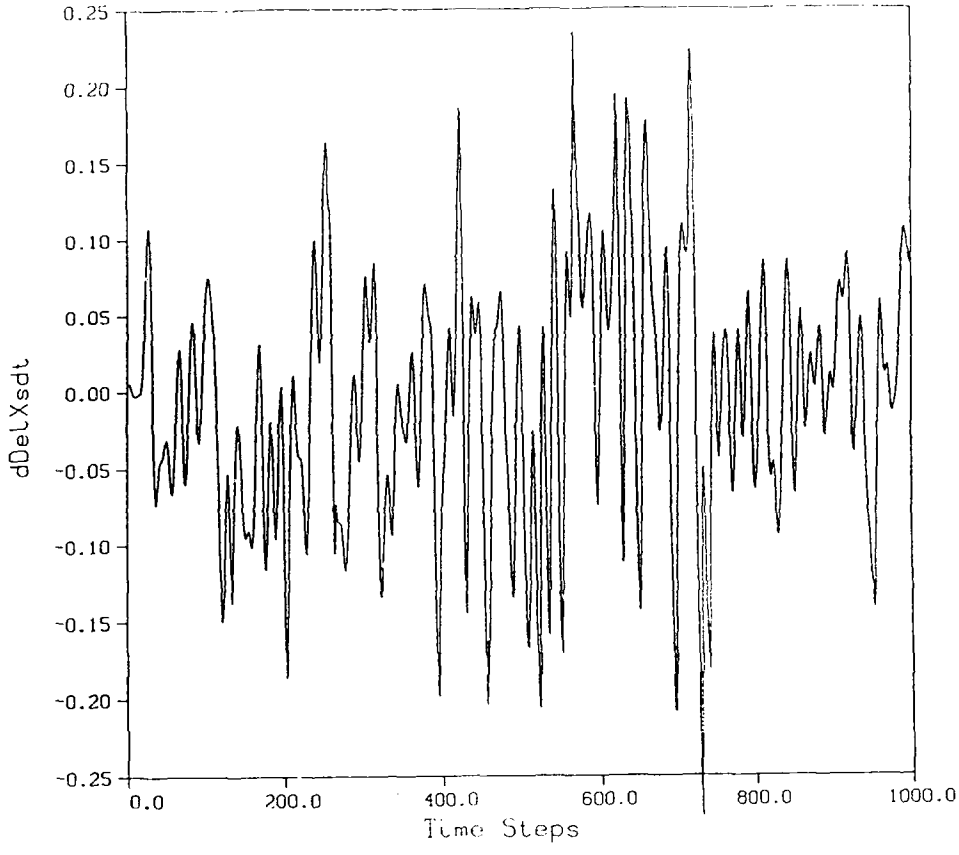

Figure B8. Plot of U_s from Navier-Stokes solution.

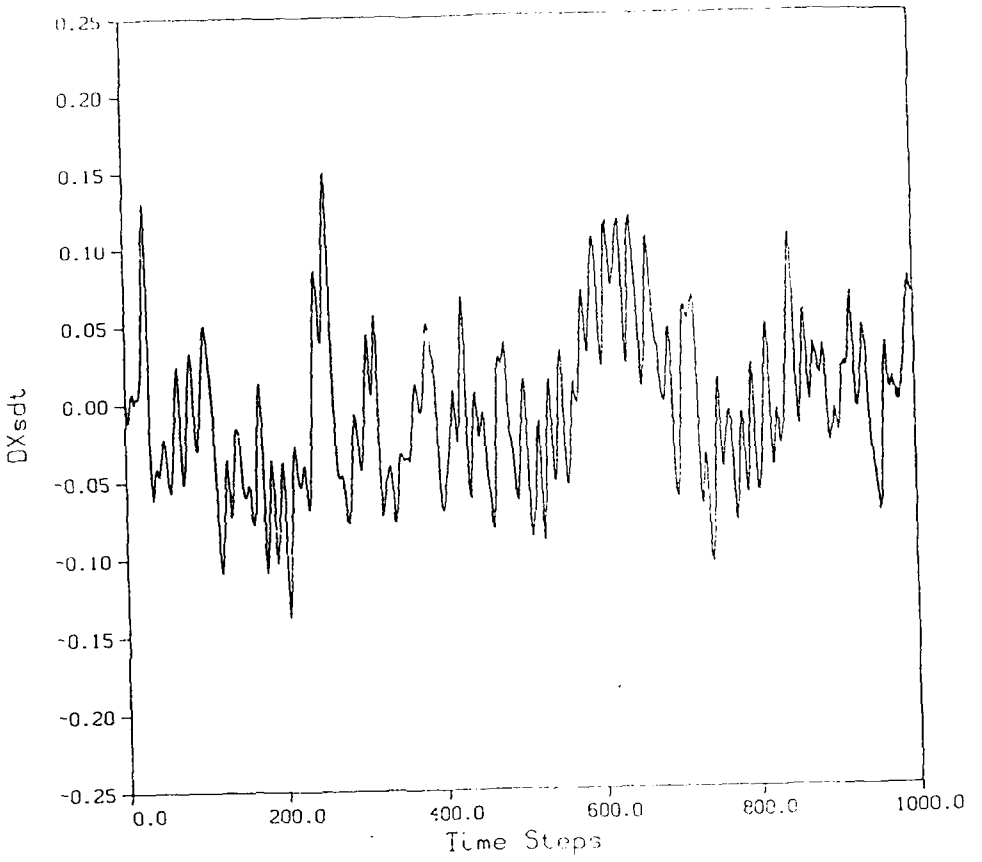

Figure B9. Plot of U_s from indicial integral.

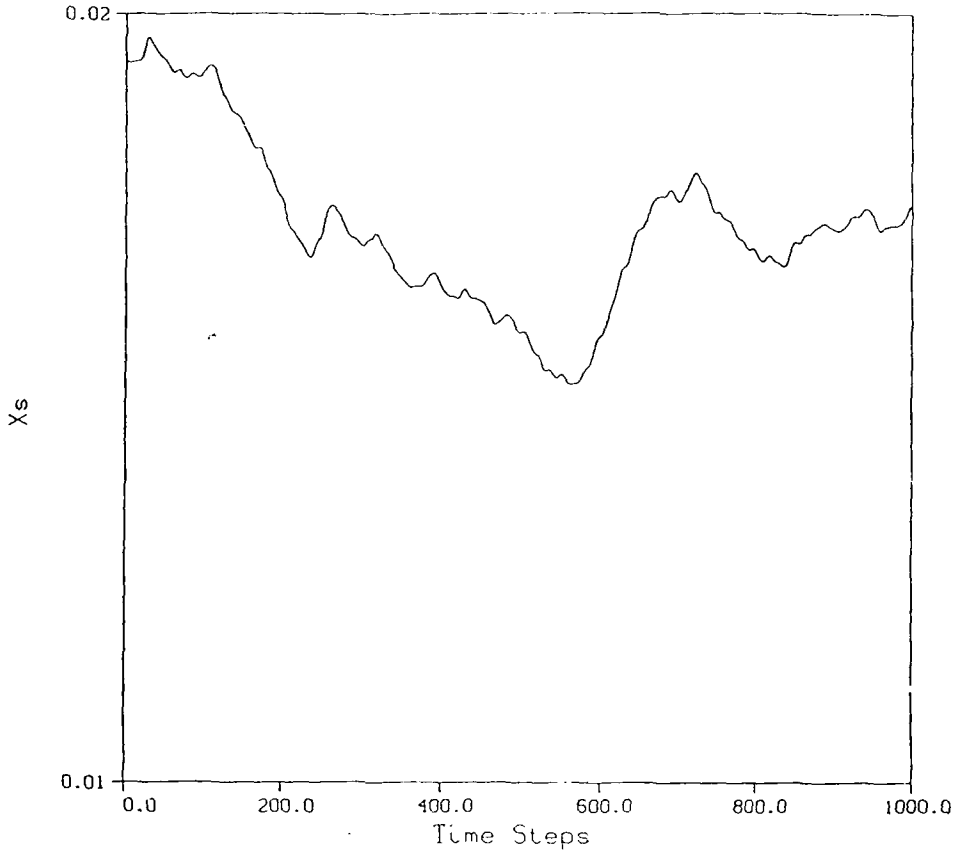

Figure B10. Plot of X_s integrated from U_s from indicial integral.

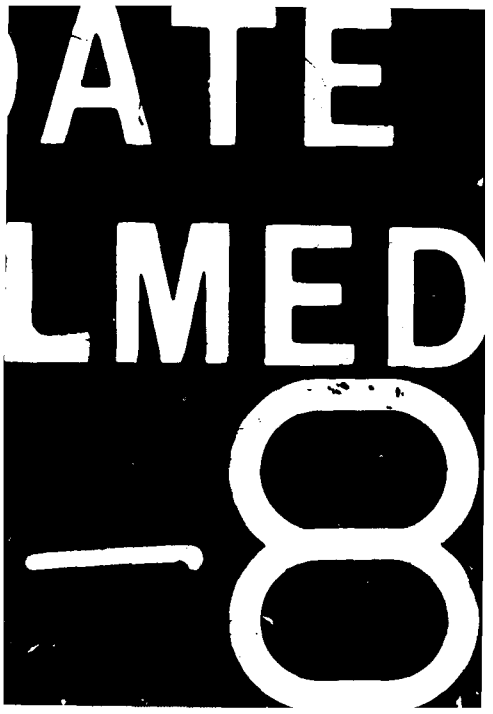
ATE
LMED
8